Clim. Past Discuss., doi:10.5194/cp-2017-10, 2017
Manuscript under review for journal Clim. Past
Published: 31 January 2017

Holocene climatic evolution at the Chinese Loess Plateau: testing sensitivity to the global warming-cooling events

Taslima Anwar[1,2], Vadim A. Kravchinsky[1,2*], Rui Zhang[1,2,3,*], Lioudmila P. Koukhar[2], Lirong Yang[1], Leping Yue[1,3]

[1] State Key Laboratory of Continental Dynamics, Department of Geology, Northwest University, Xi'an 710069, China

[2] Department of Physics, University of Alberta, Edmonton, Alberta, Canada T6G 2E1

[3] State Key laboratory of Loess and Quaternary Geology, Institute of Earth Environment, Chinese Academy of Sciences, Xi'an 710075, China

[*] *Correspondence to:* Vadim A. Kravchinsky (vadim@ualberta.ca) and Rui Zhang (zhangrui2000@qq.com)

Climate of the Past

Clim. Past Discuss., doi:10.5194/cp-2017-10, 2017
Manuscript under review for journal Clim. Past
Published: 31 January 2017

Abstract

A high resolution petromagnetic and sedimentary grain size analyses demonstrate that pedogenic alterations in the Holocene loess sequences from the region of the Guanzhong Basin and the Mu Us Desert of the Chinese Loess Plateau were affected by the climatic variations in temperature and precipitation, but not by the climatic variations of wind intensity. Three warm-humid intervals (~8.4–3.7 ka, ~2.4–1.2 ka, and ~0.81–0.48 ka), associated with the soil formation and relatively high values of petromagnetic parameters, occurred during the Holocene. A significant paleosol development from ~8.4 to 3.7 ka, along with the higher values of proxy parameters, indicates a generally strong warm-humid phase in the mid-Holocene which can be attributed as the Holocene optimum in the studied regions. The study demonstrates that the Holocene climate in China is sensitive to the large warming and cooling events and insensitive to millennial scale climate changes. A complete Holocene climate record is constructed, and that correlates well with the other regional climate records along the south-to-north of eastern Chinese loess plateau, suggesting that similar climatic pattern of changes occurred in the eastern monsoonal China during the Holocene. Results are supported by the other evidence of climate record in different regions of the world, implying the Holocene climatic optimum took place at the same time interval all over the northern hemisphere, and thus, our results correspond to global climate records as well.

Keywords: climate change; Chinese loess-paleosol sequence; environmental changes; Holocene; magnetic susceptibility; petromagnetism; soil

Clim. Past Discuss., doi:10.5194/cp-2017-10, 2017
Manuscript under review for journal Clim. Past
Published: 31 January 2017

1. Introduction

Many paleoclimate studies have underlined the climate fluctuations in the Holocene interval in many places (Steig, 1999, Bianchi and McCave, 1999; Wurster and Patterson, 2001; Baker et al., 2001; McDermott et al., 2001 and others). Studies have explored six such fluctuations across the globe with an indication of polar cooling, tropical aridity, and significant atmospheric deviations (Mayewski et al., 2004). Although the development of the current human civilization has been nurtured by the Holocene climate, there is quite a limited knowledge on climate variability during this period. However, this limitation can be addressed through the approach of comprehensive paleoclimate data collecting from different locations of the globe, particularly from the climate sensitive ones. The arid and semi-arid China provides a highly sensitive and profound area for large-scale climatic variations (Thompson et al., 1989; Feng et al., 1993; D'Arrigo et al., 2000; Jacoby et al., 2000).

Scientists and researchers have been investigating the Holocene paleoclimates and paleoenvironments of the Chinese arid zone for quite a long time (Zhu et al., 1982; Liu, 1985; An et al., 2000; Xiao et al., 2004; Feng et al., 2006; Zhou et al., 2010 and others). For this, various records and archives including pollen and loess stratigraphy, variations in level of sea and lake, lacustrine sediments and ice cores with steady isotopes have been being studied and correlated to reconstruct the climatic variation in the Holocene. Particularly, pollen data, fossil fauna, paleosol, lake level, glacial remains, and archaeological data in China considered the mid Holocene (ca. 9.4–3.1 ka) to be the Holocene optimum (Shi et al., 1992; Li, 1996). In Inner Mongolia, strong monsoon fluctuations have been recorded as glacial advance and cessation of paleosol development (Zhou et al., 1991). Based on the analyses of various records of paleoclimatic imprints or proxies, He et al. (2004) suggested that the Holocene optimum occurred at ca. 6.5–5.5 ka in the eastern China. For each area in China, the Holocene climate had three distinct phases, and the middle Holocene optimum (8–5 ka) occurred in arid to semi-arid areas (Feng et al., 2006). Studying independent proxies including contemporary pollen data, Herzschuh (2006) explored that the event of the Holocene optimum with high precipitation happened in a different time period in the Indian monsoon and the East Asian monsoon region; it is the early Holocene and the mid-Holocene respectively for these regions. In the northwest China, multi-proxy analyses indicate that a dry climate with high variation occurred from 7.8 to 1 ka (Zhao et al., 2010). As there has been a discourse among the Quaternary scientists on the climatic variations in China in different intervals of the Holocene, it requires more clarification and better understanding of this climate change through the detailed records from various sources.

Selecting proper proxies and developing reliable chronologies is the key problem in reconstructing the variations in climate and environment during the Holocene. In arid and semi-arid regions, loess-paleosol sequences react to climatic variations, indicating that these areas are suitable for investigating the evolutions of paleoclimate and paleoenvironment (Rutter, 1992; Ding et al., 1993; Maher, 2011). These sequences can be instrumental to reconstruct climatic history of neighboring regions of the Loess Plateau through the last glacial cycle (e.g., Vandenberghe et al., 1997; Sun et al., 1999; Lu et al., 1999, 2000). It is clear that more complex Holocene loess-paleosol sequences exist, and these are attributable to fluctuations in the monsoonal climate (Zhou and An, 1994; Huang et al., 2000). The loess-paleosol records with

Clim. Past Discuss., doi:10.5194/cp-2017-10, 2017
Manuscript under review for journal Clim. Past
Published: 31 January 2017

reliable chronology are critical to understand the overall pattern of climate variations in the monsoonal China during the Holocene.

The analysis of petromagnetic properties of loess-paleosol deposits is instrumental for the interpretation of paleoclimatic conditions during the time of their accumulation. In this study, these properties, along with sedimentary grain size, are analyzed to investigate the Holocene climatic variations focusing on the loess-paleosols profiles from the region of the Guanzhong Basin and the Mu Us Desert lain in the East Asian monsoonal zone. The Guanzhong Basin is located at the southern edge of the Loess Plateau whereas the Mu Us Desert is situated at the northern part of the Plateau. Here, efforts have been made to reconstruct a regional climate and environmental changes in the Holocene recorded in the Chinese Loess; to explore the influence of temperature, precipitation, and wind strength on regional climate changes; to understand the responses of regional Holocene climate along the south-to-north eastern Chinese Loess Plateau; and to investigate whether the world and China exhibit common climate dynamics or climate change differs from region to region in the Holocene.

2. The Study Area

In this study, five aeolian sections located in two different areas, the Yaozhou in the Guanzhong Basin and the Jinjie in the Mu Us Desert, were sampled. The Yaozhou (34°53′N, 108°58′E) is situated at the Guanzhong Basin, about 60-70 km east of Xi'an city (YZ in Figure 1). At middle zone of the Yellow River valley, the Guanzhong Basin is located while having the Loess Plateau to the north and the Qinling Mountains to the south (Figure 1). The land surface in the

Clim. Past Discuss., doi:10.5194/cp-2017-10, 2017
Manuscript under review for journal Clim. Past
Published: 31 January 2017

Climate of the Past Discussions

Guanzhong Basin has been quite settled because of less erosion, and eventually, it has made the aeolian dust deposits and soil surface well-preserved during the entire Holocene period (Huang et al., 2000). In the Guanzhong Basin, numerous Holocene loess-paleosol have been studied to examine changes in vegetation at the Yaoxian (Li et al., 2003), variations in climate at the Yaoxian (Zhao et al., 2007), and cultural effect at the Qingquicun (Huang et al., 2000). Analyzing the stratigraphy and the proxy data, such sequences can provide critical information regarding the fluctuations in climate, and also, they can explore major events occurred since 11 ka BP to date (Shi et al., 1992). The present mean annual temperature shows to be 13°C while mean rainfall is around 554 mm, and these are associated with a semi-humid climate that displays a significant seasonal variations in temperature and precipitation which becomes intense in summer. Three sections were investigated from this area: one at an outcrop (YZ1), the second one at 100 m further south (YZ2), and the third one at 300 m west (YZ3) from the first one. YZ2 is at the same pit of YZ1, whereas YZ3 is at a different pit. The sequence of 5 m YZ1, 3.3 m YZ2 and 4 m YZ3 are composed of three paleosol units of Holocene age (S_0S_1, S_0S_2 and S_0S_3), interbedded with two layers of loess. The stratigraphic unit was identified through the examination of colour, texture and structure of the sediment. However, the buried soils in these sections cannot be identified very well visually, and thus, the soil layers can be confirmed through the magnetic measurements.

The Jinjie (38°44′N, 110°91′E) is located at the southeastern margin of the Mu Us Desert (JJ in Figure 1). The Mu Us Desert, being situated at the northern-central China and having sand dunes, belongs to the peripheral region of the East Asian monsoon. Currently, almost two-thirds of this desert are covered by these sand dunes (Sun, 2000). The ecosystem, in the semi-arid Mu

Clim. Past Discuss., doi:10.5194/cp-2017-10, 2017
Manuscript under review for journal Clim. Past
Published: 31 January 2017

Climate of the Past Discussions

Us Desert, exhibits high sensitivity towards climate change since external climatic forces can easily affect the vegetation, soil, and aeolian sand (Sun et al., 2006). The local mean annual temperature, currently, varies from 6.0° to 9.0°C, and it is 200-400 mm in case of the mean rainfall. 70% of the rainfall concentrates from July to September, with a warm and humid summer as well as autumn. In winter, it is cold and dry with the prevailing cold winds being northwesterly. Two sections from this area, JJ1 and JJ3 (along the road and about 1 km southeast from JJ1), were studied. The 7m deep JJ1 and 8m deep JJ3 aeolian sequences contain three distinctive dark brown sandy loam soil layers (S_0S_1, S_0S_2 and S_0S_3) separated by sand beds. The stratigraphic subdivision was made by the field observation of colour, texture, and structure of the sediment. For JJ3 section, there are mixture of sand and soils in between two soil layers. All of these sections are situated above the Malan loess (L1).

The Yaozhou and the Jinjie loess paleosol sequences are both dated using optically stimulated luminescence (OSL) dating technique (Zhao et al., 2007; Ma et al., 2011). In the Yaozhou, the boundary between the lowest paleosol (S_0S_3) and the Malan Loess was OSL dated 8.44 ± 0.59 ka (Zhao et al., 2007). At the Jinjie, the lowest paleosol (S_0S_3) was bracketed by two OSL dates– 7.07 ± 0.42 ka at the bottom and 3.91 ± 0.18 ka at the top (Ma et al., 2011). Ages of each soil section are assigned based on the OSL dating of Zhao et al. (2007) for the Yaozhou area and Ma et al. (2011) for the Jinjie area.

Clim. Past Discuss., doi:10.5194/cp-2017-10, 2017
Manuscript under review for journal Clim. Past
Published: 31 January 2017

3. Methods

3.1 Sampling

A total of 573 non-oriented bulk samples were collected from the 5 sections (YZ1: 100, YZ2: 80, YZ3: 85, JJ1: 150 and JJ3: 158 samples) for petromagnetic and sedimentary grain size analyses. Samples were taken continuously at 5 cm intervals (2.5 cm intervals only for the thin soils) from all sections. Sampling was started from the top that contains present day soil i.e. the cultivated layer.

3.2 Thermomagnetic and hysteresis data

Temperature dependent magnetic susceptibility (MS) was measured on several samples from each section to investigate the magnetic mineralogy. The measurement was performed using a Bartington susceptibility meter in the Laboratory of Paleomagnetism and Petromagnetism of the Physics Department at the University of Alberta. The sample was heated up to 700°C and then allowed to cool back to room temperature in air. During heating and cooling, magnetic susceptibility measurement of the sample was taken at every 2°C. The magnetic grain size of the samples was investigated by hysteresis measurements at room temperature with a maximum field of ±1T using a VFTB in the Environmental Magnetism Laboratory, Geophysics Institute in Beijing, China. Saturation magnetization (Ms), remanent saturation magnetization (Mrs), coercive force (Hc), and the coercivity of remanence (Hcr) values were evaluated from the hysteresis loops.

3.3 Petromagnetic parameters

A number of petromagnetic parameters such as low and high frequency magnetic susceptibility, anhysteric remanent magnetization (ARM), saturation isothermal remanent magnetization (SIRM), and back field isothermal remanent magnetization (bIRM) were measured to identify variations in the concentration, grain size and mineralogy of magnetic material in the samples. These were conducted in the paleomagnetism and petromagnetism laboratory of the University of Alberta. These parameters (low field mass specific magnetic susceptibility χ_{lf} and SIRM) and the ratios derived from them (frequency dependence of magnetic susceptibility FD and normalized to the steady field anhysteric remanent magnetization (χ_{ARM})) were used to interpret the paleoclimatic conditions during deposition of the studied loess-paleosol sections.

In the laboratory, 8 cm^3 plastic non-magnetic boxes were used to host the sediments for petromagnetic measurements. The low-frequency (0.43 kHz) and high-frequency (4.3 kHz) magnetic susceptibility of each sample were measured using a Bartington Instruments MS2B dual frequency meter. To reduce the level of considerably high noise from the Bartington instrument, special precaution was taken during measurements. Each sample was measured three times in different positions, and the average MS value was calculated for both low and high frequency measurements. All the values were checked before getting the average, and found consistent without high errors. Air measurements were taken in between two samples' measurement each time to monitor and eliminate the instrumental drift. The FD value was calculated for each sample using its averaged low and high frequency MS values. ARM was acquired in the samples subjecting to a peak AF field of 100 mT and a steady DC field of 0.1 mT by a 2G cryogenic magnetometer demagnetizer. This ARM was normalized to the steady field to

Clim. Past Discuss., doi:10.5194/cp-2017-10, 2017
Manuscript under review for journal Clim. Past
Published: 31 January 2017

yield χ_{ARM}. SIRM was acquired in the samples by subjecting them to a field of 0.6 T through a 2G IRM stand-along electromagnet. bIRM was induced to the samples by using a reversed field of 0.3 T and the acquired remanences were measured on the cryogenic magnetometer. Parameters (χ_{ARM}/χ_{lf} and $\chi_{ARM}/SIRM$) were also evaluated for each sample.

3.4 Sedimentary grain size

Sedimentary grain size analysis was performed in order to determine relative wind strengths during loess deposition of the studied sections. Sedimentary grain size was measured on a Mastersizer 2000 laser particle analyzer at the Northwest University in Xian, China. The grain size samples were subjected to standard chemical pretreatment. To eliminate the organic material, samples of 0.3–0.4 g were fully dissolved in 10 ml of 10% boiling hydrogen peroxide (H_2O_2) solution in a 200 ml beaker. The carbonates were also removed by boiling with 10 ml of 10% hydrochloric acid (HCl). Distilled water was added during the chemical treatment to avoid drying of the solution. After standing overnight, the clear water was decanted from the sample. Through a combination of an addition of 10 ml of 10% sodium hexametaphosphate [$(NaPO_3)_6$] solution and an oscillation for around 10 minutes ultrasonically, dispersion was created for the components.

Clim. Past Discuss., doi:10.5194/cp-2017-10, 2017
Manuscript under review for journal Clim. Past
Published: 31 January 2017

4. Results

4.1 Thermomagnetic and hysteresis

Typical examples of temperature dependent magnetic susceptibility curves and hysteresis loops are presented in Figure 2. The MS shows decrease in the signal and reaches minimum value at approximately 590°C, indicating the presence of magnetite (Figure 2). The MS values start to increase above 590°C suggesting that hematite is produced by the oxidation of magnetite, as expected in such experiments while conducting in air. The shape of the hysteresis loops indicates samples contain pseudo-single domain (PSD) particles (Figure 2). The remanence ratio (Mrs/Ms) versus coercivity ratio (Hcr/Hc) is shown on a Day plot (Dunlop, 2002) in Figure 3. The Day plot represents that magnetic grain size of samples mainly clusters within the pseudo-single domain (PSD) region (Figure 3).

4.2 Petromagnetic parameters

The measured parameters of five sections (YZ1, YZ2, YZ3, JJ1, and JJ3) have been plotted against depth of the sections in Figure 4-8. Magnetic susceptibility has been widely used as a proxy indicator to investigate Quaternary climate change by loess-paleosol sequences on the Chinese Loess Plateau (Heller and Liu 1984; Balsam et al., 2004). The MS record demonstrates intensity variations of the pedogenesis, caused by precipitation changes related to summer monsoon climatic fluctuations (An et al., 1991; An and Xiao, 1990). χ_{lf} measures the magnetic response caused by magnetic remanences as well as non-remanent components present in the samples (Robinson, 1986; Thompson and Oldfield, 1986; Evans and Heller, 2003). χ_{lf} values (average 0.13×10^{-6} m^3kg^{-1}) for the Jinjie area (JJ1 and JJ3 sections) are relatively lower than that (average 1.05×10^{-6} m^3kg^{-1}) of the Yaozhou area (YZ1, YZ2 and YZ3 sections), suggesting that the latter area has higher concentration of magnetic particles. The loess and paleosol layers are all clearly identifiable in the χ_{lf} profiles from all sections (Figure 4-8). In this study, the susceptibility curves (χ_{lf}) of all the sections show that the soils have higher susceptibility compared to the loess/sand beds (Figure 4-8), indicating warm-wet climate conditions during the formation of these accretionary soils. On the other hand, lower χ_{lf} values in the loess/sand layers exhibit a cool-dry climate and intensified aeolian dust deposition as well as weak pedogenic processes during loess deposition. The upper layer of the soils (S_0S_1), formed thinner in a shorter period, shows weak χ_{lf} values almost as same as the values of adjacent aeolian loess/sands, whereas the lower layers of soils represent stronger signals for the sections YZ2, YZ3, JJ1, and JJ3 (Figure 5-8). For YZ1 section, S_0S_1 shows high peak with disturbance, probably due to the close proximity of S_0S_1 to the modern soil or the cultivated layer (Figure 4).

The FD parameter appears to be higher in soil horizons compared to the loess as it is related to the distribution of ferromagnetic minerals, commonly superparamagnetic magnetite produced during soil formation (Thompson and Oldfield, 1986; Evans and Heller, 2003). All soil horizons exhibit higher FD values (ranging around 8-10%) compared to their respective parent loess horizons, and these are in agreement with the χ_{lf} values (Figure 4-7). These higher FD values of studied soil horizons confirm the continuous production of superparamagnetic particles during the pedogenesis in warmer interval. However, for the JJ3 section, the FD parameter does not show variations to corresponding sands and soils (Figure 8), probably due to the sandiness of the soils for this section.

Clim. Past Discuss., doi:10.5194/cp-2017-10, 2017
Manuscript under review for journal Clim. Past
Published: 31 January 2017

χ_{ARM} and SIRM indicate variations in magnetic mineral concentration, and values get higher with increasing concentration of minerals having a high magnetization such as magnetite (Thompson and Oldfield, 1986; Yu and Oldfield, 1989; King and Channell, 1991; Evans and Heller, 2003). Figure 4-8 indicate that the paleosol horizons have higher χ_{ARM} and SIRM values compared to the loess/sand horizons. The higher χ_{ARM} and SIRM values represent higher concentration of magnetic particles within the soil layers, and indicate warmer-wetter conditions and active pedogenic processes during the time of soil formation. Whereas lower values, found in the loess/sand layers, indicate cooler-drier conditions and weak pedogenic intensity during the periods of intensified dust deposition. For all the sections, χ_{ARM} and SIRM curves indicate the presence of χ_{lf} and FD peaks, corresponding to the soil horizons (Figure 4-8).

4.3 Sedimentary grain size

The grain size variations of loess deposits have commonly been used to monitor past wind intensity changes (Pye and Zhou, 1989; Rea, 1994). Stronger winds are associated with more dust storms, coarser particle size and larger dust input to the Loess Plateau (Ding et al., 1994). The average median grain size values are larger for the Jinjie area (~ 220 μm) than the Yaozhou area (~ 13.9 μm), representing that the grain size records of the Holocene loess deposits decrease from north to south over the Chinese Loess Plateau. The grain size of the last glacial loess deposits also displays an overall southward decrease (Yang and Ding, 2004) as the loess was created primarily in the sandy Gobi deserts in northwestern China and was carried away by the near-surface northwesterly wind (Liu 1985; An et al., 1991). The median grain size of the studied sections does not demonstrate well the general characteristic of the smaller values for the soil horizons (Figure 9-13), indicating that the wind intensity did not vary much for these areas during the Holocene. Moreover, the median grain size of the loess and soil horizons of the Yaozhou area (YZ1, YZ2 and YZ3 sections) shows a little variability (Figure 9-11) compared to the loess and soil layers of the Jinjie area (JJ1 and JJ3 sections) (Figure 12-13), suggesting that the wind intensity fluctuation was higher in the north loess plateau (Jinjie area) in contrast with the south loess plateau (Yaozhou area).

The ratios χ_{ARM}/χ_{lf} and $\chi_{ARM}/SIRM$ indicate variations in magnetic grain size and the values decrease with increasing magnetic grain size (Thompson and Oldfield, 1986; King et al., 1982; Maher, 1988; Evans and Heller, 2003). For all the sections, magnetic grain size (χ_{ARM}/χ_{lf} and $\chi_{ARM}/SIRM$) varies in the same manner as the sedimentary grain size does (Figure 9-13). Both the ratios reflect a little variability for loess and soil horizons indicating smaller relative changes in magnetic grain sizes.

5. Discussion

5.1 Variations in the Holocene climate

Three soil layers (S_0S_1, S_0S_2 and S_0S_3) are identified for all the sections not only in the field but also in the laboratory by higher magnetic concentration parameters (χ_{lf}, χ_{ARM}, SIRM) and FD parameter. Therefore, χ_{lf}, FD, χ_{ARM} and SIRM are higher for soil and lower for loess/sand horizons, indicating warmer and colder assemblage respectively. The sedimentary and magnetic grain size variations do not correspond to the soil intervals entirely. Furthermore, the magnetic concentration parameters and FD parameter show a larger variation for the loess and soil layers compared to the sedimentary and magnetic grain sizes for these layers. It demonstrates that humidity fluctuation, which is related to the vegetation and soil formation, was stronger than the wind intensity variation for the studied sections during the Holocene.

Petromagnetic analysis of five loess sections in the Yaozhou and the Jinjie areas shows clear changes in regional climate, and provides paleoenvironmental information over the Holocene. Changes of parameters with soil formation in five studied sections, at the Yaozhou (Jinjie), suggests three distinct warm-humid time periods during the Holocene: the oldest warmer interval was between 8.4–3.7 ka (7.0–3.9 ka), the middle one occurred between 2.4–1.2 ka (2.9–1.7 ka), and the youngest started at 0.81 ka (1.1 ka) (Figure 4-8). Furthermore, based on the data, two cold-dry intervals associated with loess deposition can be considered at the Yaozhou (Jinjie): 3.7–2.4 ka (3.9–2.9 ka) and 1.2–0.81 ka (1.7–1.1 ka). However, at these areas, the onset and termination of warming-cooling intervals during the Holocene were almost similar with a slight difference. A subsequent warm-humid phase took place between ~8.4 ka and ~3.7 ka, indicated by the development of strong soil (S_0S_3) in all five sites. Combined with high values of all petromagnetic parameters in the studied regions (Figure 4-8), this period is attributed to the Holocene optimum, a warm period (generally warmer than today) in the middle of the Holocene. Soil S_0S_3 formation terminated around ~3.7 ka, suggesting a cold-arid period. This resulted in an active period for the loess/sand during ~3.7–2.4 ka. The soil S_0S_2 developed between ~2.4 and ~1.2 ka, and at that time, the values of the petromagnetic parameters indicate a warm-humid period in this region (Figure 4-8). The climate became colder and drier between ~1.2 and ~0.81

Clim. Past Discuss., doi:10.5194/cp-2017-10, 2017
Manuscript under review for journal Clim. Past
Published: 31 January 2017

ka as the sand/loess was deposited, illustrated by low values of petromagnetic parameters. Soil S_0S_1 formed in the interval of ~0.81–0.48 ka (Figure 4-8), suggesting a warm-humid period.

5.2 Comparison of regional paleoclimatic records

Changes in climate in the studied sections can be compared with the other reported paleoclimatic records from the neighboring monsoonal region of semi-arid China. In this study, we used tree pollen records from peatlands or lakes, located along the south-to-north regional transect on the eastern Loess Plateau, to make comparison with our results. In order to compare, low frequency magnetic susceptibility (χ_{lf}) of YZ3 section from the Yaozhou and JJ3 section from the Jinjie have been selected as reference curve since these identify soil intervals better than the others. The sites from south to north include the Hongyuan peatland (Zhou et al., 2010), the Yaozhou (YZ3), the Jinjie (JJ3), the Daihai Lake (Xiao et al., 2004), and the Hulun Lake (Wen et al., 2010) (Figure 1 and 14). Summer temperature and precipitation are two dominant climatic factors controlling soil formation as well as pollen assemblages (Shen et al., 2006). Thus, high magnetic parameters and high tree pollen should reflect warm-wet climates. Three warmer intervals of the studied region visually correlate well with the higher pollen data (Figure 14).

Pollen records from the Hongyuan peatland (Zhou et al., 2010), the Daihai Lake (Xiao et al., 2004), and the Hulun Lake (Wen et al., 2010) show peak tree pollen abundance in the mid-Holocene between ~8.4 and ~3.7 ka (Figure 14), suggesting a warmer-wetter climate. There is an agreement in the mid-Holocene maximum or climate optimum as documented at our studied sections and other sites (Figure 14). In the Lake Daihai which is situated at the northeast from the

Mu Us Desert, high and stable lake level also occurred at ~8–3 ka (Sun et al., 2009). An ancient wetland existed continuously from ~7.8 to 4 ka at valleys, southeast of the Lanzhou, which is located further west from the Yaozhou (An et al., 2005). A humid mid-Holocene corresponds well with a more recent reconstruction of monsoonal precipitation through various imprints from the Chinese Loess Plateau (Lu et al., 2013). Zhao and Yu (2012) studied most of the sites of the temporary zone, located between forest and temperate steppe vegetation in the northeastern China, and confirmed the presence of the wettest climate occurred between ~8 and ~4 ka. The high level of the Lake Huangqihai during 8–4 ka (Shen, 2013), situated in the monsoonal region, indicates a strong East Asian summer monsoon happened in the mid-Holocene. In the Horqin dunefield, the greater density of vegetation coverage occurred between ~8 and ~3.2 ka, suggesting a warm and humid climate (Mu et al., 2016). Even though the termination of the warm-humid Holocene optimum slightly vary in different sections, this is possibly due to the age model imperfections and assumptions of the close to constant sedimentation rate, the inconsistencies of various of different dating methods or irregularity of the Holocene optimum (e.g., An et al., 2000; He et al., 2004).

From ~3.7 to ~2.4 ka, the decreasing susceptibility of the studied sections suggests a drying and cooling climate trend that correlates with the tree pollen data (Figure 14). The pollen sequence collected from the Taishizhuang peat site, located at the southeastern edge of the Mongolian Plateau, confirms a significant climatic variation taken place at around ~3.4 ka, and during that time, the tree component almost disappeared entirely (Jin and Liu, 2002; Tarasov et al., 2006). Both in the south-central and the southeastern Inner Mongolia region, a major cultural shift occurred at ~3.5 ka (Liu and Feng 2012). After ~3.7 ka, aeolian sand transportation took place more frequently and the East Asian summer monsoon strength decayed significantly, as perceived from the higher probability density values (Wang et al., 2014). A drying and cooling climatic shift also found in two cave speleothem sequences in the southern China from the Linhua Cave at ~3.3–3.0 ka (Cosford et al., 2008), and from the Heshang Cave at ~3.6–3.1 ka (Hu et al., 2008).

For the interval of ~2.4–1.2 ka, the magnetic climate data of this study coincides well with the tree pollen data of the Hongyuan peatland (Zhou et al., 2010), the Daihai Lake (Xiao et al., 2004), and the Hulun Lake (Wen et al., 2010) (Figure 14). This period can be confirmed by the moist grassland at the Guanzhong Basin (Li et al., 2003). Furthermore, in Figure 14, the correlation analysis of magnetic susceptibility and tree pollen data shows good agreement for the cold-dry interval of ~1.2–0.81 ka. Although the warmer interval of ~0.81–0.48 ka, recorded by the magnetic proxies in this study, does not correlate well with the tree pollen data of the Hongyuan peatland (Zhou et al., 2010) and the Hulun Lake (Wen et al., 2010), however, it shows a good agreement with the tree pollen data of the Daihai Lake (Xiao et al., 2004) (Figure 14). Our results are in broad agreement with pollen records, and demonstrate that same climatic variation occurred along the south-to-north eastern Chinese Loess Plateau during the Holocene.

5.3 Comparison of global paleoclimatic records

Our results of Holocene climate changes in China can be compared with the global records. We compare our low frequency magnetic susceptibility (χ_{lf}) records of YZ3 and JJ3 sections with the Lake Baikal $\delta^{18}O$ values from diatom silica (Mackay et al., 2011), FD records of the

Clim. Past Discuss., doi:10.5194/cp-2017-10, 2017
Manuscript under review for journal Clim. Past
Published: 31 January 2017

Burdukovo loess section in Siberia (Kravchinsky et al., 2013), temperature variations in the northern hemisphere (McMichael, 2012), and Drift Ice Indices Stack from the North Atlantic (Bond et al., 2001) (Figure 15). Temperature variations in the northern hemisphere during the Holocene have been reconstructed through the average of various published data (McMichael, 2012). The studied major episodes correspond visually to the other global records (Figure 15).

For ~8.4–3.7 ka, our data show high susceptibility and indicate warm-humid period for the whole interval. Whereas, $\delta^{18}O$ values of the Lake Baikal (Mackay et al., 2011), FD values of the Burdukovo loess section (Kravchinsky et al., 2013), temperature variations in the northern hemisphere (McMichael, 2012), and Drift Ice Indices Stack from the North Atlantic (Bond et al., 2001) show two peaks during that interval (Figure 15). The higher latitude section Burdukovo resolves short-term climate variations. The Lake Baikal record sampling resolution is quite low, but it also registers the cooling interval between ~5 and 6 ka very well. There exists no clear indication of such cooling interval in the studied Chinese loess sections. It may be due to the reason that the high latitudes are more sensitive to the millennial scale changes in the orbital parameters than the southern latitudes as demonstrated by the analysis in Loutre et al. (1992). Although a couple of studies indicate millennial scale Holocene climate variations in northwest China (Yu et al., 2006; Zhao et al., 2010; Yu et al., 2012), we find that the Holocene climate is insensitive to these variations in our studied regions. Usoskin et al. (2007) suggested the probability of the effect of the orbital parameters of the Earth's climate being insignificant in clarifying the direct influence of solar variability on climate change. Beer et al. (2006) examined the probable feedback mechanisms for the amplification of the solar heating effect. Nevertheless, the whole interval of ~8.4–3.7 ka in China can be considered warm and humid period. The period between ~7 and 4.2 ka BP was demonstrated as high summer temperature in the mid and high latitude areas of the northern hemisphere (Klimenko et al., 1996; Alverson et al., 2003). Furthermore, an extensive paleosol, developed on the eastern belt of the Badain Jaran Desert, indicates a climate optimum in the mid Holocene (Yang et al., 2011). This humid episode between ~8.4 ka and ~3.7 ka is also found in the North Africa (Guo et al., 2000). Therefore, the interval of ~8.4–3.7 ka can be considered a globally registered Holocene optimum period.

A cool and dry climate from ~3.7 to ~ 2.4 ka caused the lowest χ_{lf} and well-preserved loess/sand in the studied area, also indicated by other global data (Figure 15). A cold and arid period from ~3.5 to ~2.5 ka in the northern hemisphere was determined by Mayewski et al. (2004), and this interval is almost the same arid period as found in this study. In the northern hemisphere, the 3.5–2.5 ka shows rapid climate change intervals including the North Atlantic ice-rafting events (Bond et al., 1997), and strengthened westerlies over the North Atlantic and Siberia (Meeker and Mayewski, 2002). The interval, at 3.5–2.5 ka, also presents a strong aridity in the regions like the East Africa, the Amazon Basin, Ecuador, and the Caribbean/Bermuda region (Haug et al., 2001). Wanner et al. (2011) reviewed that the global cooling event between ~3.3 and ~2.5 ka coincided with a considerably low solar activity forcing.

In Figure 15, warmer interval of ~2.4–1.2 ka and colder interval of ~1.2–0.81 ka in the studied area correlate well with the $\delta^{18}O$ values of the Lake Baikal (Mackay et al., 2011), FD values of the Burdukovo loess section (Kravchinsky et al., 2013), temperature variations in the northern hemisphere (McMichael, 2012), and Drift Ice Indices Stack from the North Atlantic (Bond et al., 2001). This event (~1.2 to 1.0 ka) corresponds to the maxima in the $\delta^{14}C$ and ^{10}Be records,

Clim. Past Discuss., doi:10.5194/cp-2017-10, 2017
Manuscript under review for journal Clim. Past
Published: 31 January 2017

indicating a weakening in solar output at this interval (Mayewski et al., 2004). At low latitudes, ~1.2–1.0 ka usually shows dry conditions in the tropical Africa and the monsoonal Pakistan (Gasse, 2000; 2001). During ~1.2 to 1.0 ka, atmospheric CO_2 surged moderately and caused variations in solar output resulting in drought in the Yucatan (Hodell et al., 1991, 2001). The other warmer interval of ~0.81–0.48 ka also corresponds to FD parameter in the Burdukovo (Kravchinsky et al., 2013), temperature variations in the northern hemisphere (McMichael, 2012), and Drift Ice Indices Stack from the North Atlantic (Bond et al., 2001). However, the resolution of the $\delta^{18}O$ data from the Holocene sediments of the Lake Baikal is not very high (Mackay et al., 2011), and does not allow to evaluate this interval in the Lake Baikal.

Our results demonstrate that changes in petromagnetic parameters of the loess-paleosol sequences in the studied area correlate closely with variations in climate documented separately, as explored by other proxies. Such correspondence demonstrates the global connections among the continental climate in Asia and the central Eurasia, temperature variations in the northern hemisphere, and the oceanic climate of the North Atlantic. Furthermore, the Holocene optimum period (~8.4 to 3.7 ka) in the studied regions, indicating a stronger warm-wet phase, appears to be a globally registered warming period.

6. Conclusions

(1) Petromagnetic and grain size analyses provide evidence for pedogenic alteration in the Holocene loess sequences of the Chinese Loess Plateau, affected by the climatic variation in temperature and precipitation but not by the climatic variation of wind intensity.

(2) Results indicate that subsequent warm-humid phase occurred in the studied regions during ~8.4–3.7 ka, ~2.4–1.2 ka, and ~0.81–0.48 ka, evidenced by the development of paleosols as well as high values of petromagnetic parameters in all sections.

(3) The Holocene climatic optimum period, in the studied regions, occurred between ~8.4 and ~3.7 ka. This climate shows sensitivity to the large warming and cooling events while being insensitive to millennial scale climate changes.

(4) The Holocene climate record of the studied regions is consistent with the reported climate records from the tree pollen analysis along the south-to-north eastern Chinese Loess Plateau at that time, suggesting that that same climatic variation occurred in the eastern monsoonal China.

(5) Our results correspond to the record of climate changes on regional and/or global scales, implying that similar climatic pattern of changes occurred in different regions of the world during the Holocene and the Holocene climatic optimum took place at the same time interval all over the northern hemisphere.

Acknowledgements

We thank Jiao J. for his support in laboratory measurement. This study was funded by the Department of Geology at the Northwest University (Xian, China) and Natural Sciences and Engineering Research Council of Canada (NSERC) for V.A.K., and the National Science Foundation of China for R.Z.

Clim. Past Discuss., doi:10.5194/cp-2017-10, 2017
Manuscript under review for journal Clim. Past
Published: 31 January 2017

Data availability

We release the data presented here to the public domain at https://www.pangaea.de/.

Clim. Past Discuss., doi:10.5194/cp-2017-10, 2017
Manuscript under review for journal Clim. Past
Published: 31 January 2017

References

Alverson, K.D., Bradley, R.S., Pedersen, T.F., 2003. Paleoclimate, Global Change and the Future. Springer, New York.

An, Z.S., Xiao, J.L., 1990. Study on the eolian dust flux over the Loess Plateau – an example. Chin. Sci. Bull., 35, 1627–1631.

An, Z.S., Kukla, G., Porter, S.C., Xiao, J.L., 1991. Late quaternary dust flow on the Chinese Loess Plateau. Catena, 18, 125–132.

An, Z.S., Porter, S.C., Kutzbach, J.E., Wu, X.H., Wang, S.M., Liu, X.D., Li, X.Q., Zhou, W.J., 2000. Asynchronous Holocene optimum of the East Asian monsoon. Quaternary Science Reviews, 19, 734–762.

An, C.B., Tang, L.Y., Barton, L., and Chen, F.H., 2005. Climate change and cultural response around 4000 cal yr B.P. in the western part of Chinese Loess Plateau. Quaternary Research, 63, 347–52.

Baker, P. A., Seltzer, G.O., Fritz, S.C., Dunbar, R.B., Grove, M.J., Tapia, P.M., Cross, S.L., Rowe, H.D., and Broda, J.P., 2001. The History of South American tropical precipitation for the past 25,000 years. Science, 291, 640–43.

Balsam, W., Ji, J.F., Chen, J., 2004. Climatic interpretation of the Luochuan and Lingtai loess sections, China, based on changing iron oxide mineralogy and magnetic susceptibility. Earth Planet. Sci. Lett., 223, 335–348.

Beer, J., Vonmoos, M., Muscheler, R., 2006. Solar variability over the past several millennia. Space Science Reviews, 125, 67–79.

Bianchi, G.G., and McCave, I.N., 1999. Holocene periodicity in north Atlantic climate and deep-ocean flow south of Iceland. Nature, 397, 515–17.

Bond, G., Showers, W., Cheseby, M., Lotti, R., Almasi, P., deMenocal, P., Priore, P., Cullen, H., Hajdas, I., Bonani, G., 1997. A pervasive millenial-scale cycle in North Atlantic Holocene and glacial climates. Science, 278, 1257– 1266.

Bond, G., Kromer, B., Beer, J., Muscheler, R., Evans, M.N., Showers, W., Hoffmann, S., Lotti-Bond, R., Hajdas, I., Bonani, G., 2001. Persistent solar influence on north Atlantic climate during the Holocene. Science, 294, 2130–2136.

Cosford, J., Qing, H., Eglington, B., Mattey, D., Yuan, D., Zhang, M., & Cheng, H., 2008. East Asian monsoon variability since the Mid-Holocene recorded in a high-resolution, absolute-dated aragonite speleothem from eastern China. Earth and Planetary Science Letters, 275(3), 296–307.

D'Arrigo, R., Jacoby, G., Pederson, N., Frank, D., Buckley, B., Nachin, B., Mijiddorj, R. and Dugarjav, C., 2000. Mongolian tree-rings, temperature sensitivity and reconstructions of Northern Hemisphere temperature. The Holocene, 10(6), 669–672.

Ding, Z.L., Rutter, N.W., Liu, T., 1993. Pedostratigraphy of Chinese loess deposits and climatic cycles in the last 2.5 Ma. Catena, 20, 73–91.

Ding, Z. L., Z. W. Yu, N. W. Rutter, and T. S. Liu, 1994. Towards an orbital time scale for Chinese loess deposits, Quat. Sci. Rev., 13, 39–70.

Dunlop, D.J., 2002. Theory and application of the Day plot (Mrs/Ms vs Hcr/Hc) 1. Theoretical curves and test using titanomagnetite data. J. Geophys. Res. 107, 4–22.

Evans, M.E., Heller, F., 2003. Environmental Magnetism: Principles and Applications of Enviromagnetics, Elsevier Science, Academic Press.

Feng, Z.D., An, C.B., Wang, H.B., 2006. Holocene climatic and environmental changes in the arid and semi-arid areas of China: a review. The Holocene, 16, 119–130.

Feng, Z.-D., Thompson, L.G., Mosley-Thompson, E., and Yao, T.D., 1993. Time-space model of climatic change in China during the past 10000 years. The Holocene, 3, 174–180.

Gasse, F., 2000. Hydrological changes in the African tropics since the last glacial maximum. Quaternary Science Reviews, 19, 189–211.

Gasse, F., 2001. Hydrological changes in Africa. Science, 292, 2259–2260.

Guo, Z.T., Petit-Maire, N. and Kröpelin, S., 2000. Holocene nonorbital climatic events in present-day arid areas of northern Africa and China. Global and Planetary Change, 26, 97–103.

Haug, G.H., Hughen, K.A., Sigman, D.M., Peterson, L.C., Röhl, U., 2001. Southward migration of the intertropical Convergence zone through the olocene. Science, 293, 1304–1308.

He, Y., Theakstone, W.H., Zhang, Z.L., Zhang, D., Yao, T.D., Chen, T., Shen, Y.P., Pang, H.X., 2004. Asynchronous Holocene climatic change across China. Quaternary Research, 61, 52–61.

Heller, F., Liu, T.S., 1984. Magnetism of Chinese loess deposits. Geophysical Journal of the Royal Astronomical Society, 77, 125–141.

Herzschuh, U., 2006. Palaeo-moisture evolution in monsoonal central Asia during the last 50,000 years. Quaternary Science Reviews, 25, 163–178.

Hodell, D.A., Curtis, J.H., Jones, G.A., Higuera-Gundy, A., Brenner, M., Binford, M.W., Dorsey, K.T., 1991. Reconstruction of Caribbean climate change over the past 10,500 years. Nature, 352, 790–793.

Hodell, D.A., Brenner, M., Curtis, J.H., Guilderson, T., 2001. Solar forcing of drought frequency in the Maya Lowlands. Science, 292, 1367–1370.

Hu, C., Henderson, G. M., Huang, J., Xie, S., Sun, Y., & Johnson, K. R., 2008. Quantification of Holocene Asian monsoon rainfall from spatially separated cave records. Earth and Planetary Science Letters, 266(3), 221–232.

Huang, C. C., Zhou, J., Pang, J., Han, Y., & Hou, C., 2000. A regional aridity phase and its possible cultural impact during the Holocene Megathermal in the Guanzhong Basin, China. The Holocene 10(1), 135–142.

Jacoby, G., D'Arrigo, R., Davaajamts, T.S., 2000. Mongolian tree-rings and 20th century warming. Science, 273, 771–773.

Jin, G.Y., and Liu, T.S., 2002. Mid-Holocene climate change in North China, and the effect on cultural development. Chinese Science Bulletin, 47, 408–413.

King, J.W., and Channell, J.E.T., 1991. Sedimentary magnetism, environmental magnetism, and magnetostratigraphy. Rev. Geophys., 358–370.

King, J.W., Banerjee, S.K., Marvin, J., Ozdemir O., 1982. A comparison of different magnetic methods for determining the relative grain size of magnetite in natural materials: some results from lake sediments, Earth Planet. Sci. Lett., 59, 404–419.

Klimenko, V.V., Klimanov, V.A., Fedorov, M.V., 1996. The history of the mean temperature of the Northern Hemisphere over the last 11,000 years. Trans. Russ. Acad. Sci., 4, 626–629.

Kravchinsky, V.A., Langereis, C.G., Walker, S.D., Dlusskiy, K.G. and White, D., 2013. Discovery of Holocene millennial climate cycles in the Asian continental interior: Has the sun been governing the continental climate?. Global and Planetary Change, 110, 386–396.

Loutre, M.F., Berger, A., Bretagnon, P. and Blanca, P.L., 1992. Astronomical frequencies for climate research at the decadal to century time scale. Climate Dynamics, 7(4), 181–194.

Li, J.J., 1996. Climatic change in arid areas of China and monsoon fluctuations during the past 10 kyears. Journal of Arid Environments, 32, 1–7.

Li, X.Q., Zhou, J., and Dodson, J., 2003. The vegetation characteristics of the 'Yuan' area at Yaoxian on the Loess Plateau in China over the last 12000 years. Review of Palaeobotany and Palynology, 124, 1–7.

Liu, T.S., 1985. Loess and Environment. Beijing: Science Press pp. 481.

Liu, F., & Feng, Z., 2012. A dramatic climatic transition at~ 4000 cal. yr BP and its cultural responses in Chinese cultural domains. The Holocene, 22(10), 1181–1197.

Lu, H.Y., VanHuissteden, K.O., An, Z.S., Nugteren, G., Vandenberghe, J., 1999. East Asia winter monsoon variations on a millennial time-scale before the last glacial– interglacial cycle. J. Quat. Sci., 14, 101–110.

Lu, H.Y., VanHuissteden, K.O., Zhou, J., Vandenberghe, J., Liu, X.D., An, Z.S., 2000. Variability of East Asian winter monsoon in Quaternary climatic extremes in North China. Quat. Res., 54, 321–327.

Lu, H.Y., Yi, S.W., Liu, Z.Y., Mason, J.A., Jiang, D.B., Cheng, J., Stevens, T., Xu, Z.W., Zhang, E.L., Jin, L.Y., Zhang, Z.H., Guo, Z.T., Wang, Y., Otto-Bliesner, B., 2013. Variation of East Asian monsoon precipitation during the past 21 ky and potential CO2 forcing. Geology, 41(9), 1023–1026.

Ma Ji., Yue L., Yang Li., Sun Lu, Xu, 2011. Southeastern margin of the Mu Us Desert Holocene sectional OSL's and paleoclimatic significance (in Chinese). Quaternary Research, 31 (1), 120–129.

Mackay, A.W., Swann, G.E.A., Brewer, T., Leng, M.J., Morley, D.W., Piotrowska, N., Rioual, P., White, D., 2011. A reassessment of late glacial-Holocene diatom oxygen isotope records from Lake Baikal using a mass balance approach. Journal of Quaternary Science, 26 (6), 627–634.

Maher, B.A., 1988. Magnetic properties of some synthetic submicron magnetite, Geophys. J., 94, 83–96.

Maher, B.A., 2011. The magnetic properties of Quaternary aeolian dust and sediments, and their palaeoclimatic significance. Aeolian Research, 3, 87–144.

Mayewski, P.A., Rohling, E.E., Stager, J.C., Karlén, W., Maasch, K.A., Meeker, L.D., Meyerson, E.A., Gasse, F., Kreveld, S.V., Holmgren, K., Lee-Thorp, J., Rosqvist, G., Rack, F., Staubwasser, M., Schneider, R.R. and Steig, E.J. 2004. Holocene climate variability. Quaternary Research, 62, 243–55.

McDermott, F., Mattey, D.P., and Hawkesworth, C., 2001. Centennial-scale Holocene climate variability revealed by a highresolution speleothem 5180 record from SW Ireland. Science, 294, 1328–31.

McMichael, A.J., 2012. Insights from past millennia into climatic impacts on human health and survival. Proceedings of the National Academy of Sciences, 109(13), 4730–4737.

Meeker, L.D., and Mayewski, P.A., 2002. A 1400-year high-resolution record of atmospheric circulation over the North Atlantic and Asia. Holocene, 12, 257–266.

Mu, Y., Qin, X., Zhang, L., & Xu, B., 2016. Holocene climate change evidence from high-resolution loess/paleosol records and the linkage to fire–climate change–human activities in the Horqin dunefield in northern China. Journal of Asian Earth Sciences, 121, 1–8.

Pye, K., and Zhou, L.P., 1989. Late Pleistocene and Holocene aeolian dust deposition in North China and the Northwest Pacific Ocean. Palaeogeography, Palaeoclimatology, Palaeoecology, 73, 11–23.

Rea, D. K., 1994. The paleoclimatic record provided by eolian deposition in the deep sea: The geologic history of wind, Rev. Geophys., 32, 159–195.

Robinson, S.G., 1986. The late Pleistocene paleoclimatic record of North Atlantic deep-sea sediments revealed by mineral-magnetic measurements, Phys. Earth Planet. Inter., 42, 22–47.

Rutter, N.W., 1992. Chinese loess and global change. Quat. Sci. Rev., 11, 275– 281.

Shen, J., 2013. Spatiotemporal variations of Chinese lakes and their driving mechanisms since the Last Glacial Maximum: a review and synthesis of lacustrine sediment archives. Chinese Science Bulletin, 58 (1), 17–31.

Shen, C.M., Liu, K.-B., Tang, L.Y., Overpeck, J.T., 2006. Quantitative relationships between modern pollen rain and climate in the Tibetan Plateau. Review of Palaeobotany and Palynology, 140, 61–77.

Shi, Y.F., Kong, Z.C. and Wang, S.M., 1992. Climatic variations and the major events in the Holocene Megathermal in China (in Chinese). Science in China, 12, 300–308.

Steig, E.J., 1999. Mid-Holocene climate change. Science, 286, 1485–87.

Sun, J.M., 2000. Origin of eolian sand mobilization during the past 2300 years in the Mu Us Desert, China. Quaternary Research, 53, 73–88.

Sun, J.M., Ding, Z.L., Liu, T.S., Rokosh, D., Rutter, N.W., 1999. 580,000-year environmental reconstruction from aeolian deposits at the Mu Us desert margin, China. Quat. Sci. Rev., 18, 1351–1364.

Sun, J.M., Li, S. H., Han, P., Chen, Y., 2006. Holocene environmental changes in the central Inner Mongolia, based on single-aliquot-quartz optical dating and multi-proxy study of dune sands. Palaeogeography, Palaeoclimatology, Palaeoecology, 233, 51–62.

Sun, Q.L., Wang, S.M., Zhou, J., Shen, J., Cheng, P., Xie, X.P., Wu, F., 2009. Lake surface fluctuations since the late glaciation at Lake Daihai, North-central China: a direct indicator of hydrological process responses to East Asian monsoon climate. Quaternary International, 194, 45–54.

Tarasov, P., Jin, G.Y., and Wagner, M., 2006. Mid-Holocene environmental and human dynamics in Northeastern China reconstructed from pollen and archaeological data. Palaeogeography Palaeoclimatology Palaeoecology, 241, 284–300.

Thompson, R., Oldfield, F., 1986. Environmental Magnetism, Allen and Unwin, London.

Thompson, L.G., Mosley-Thompson, E., Davis, M.E., Bolzan, J.F., Dai, J., Yao, T., Gundestrup, N., Wu, X., Klein, Z. and Xie, Z., 1989. Holocene-Late Pleistocene climatic ice core records from Qinghai-Tibetan Plateau. Science, 246, 474–477.

Usoskin, I.G., Solanki, S.K., Kovaltsov, G.A., 2007. Grand minima and maxima of solar activity: new observational constraints. Astronomy and Astrophysics, 471, 301–309.

Vandenberghe, J., An, Z.S., Nugteren, G., Lu, H.Y., VanHuissteden, K., 1997. New absolute time scale for the Quaternary climate in the Chinese loess region by grain-size analysis. Geology, 25, 35–38.

Wang, H., Chen, J., Zhang, X., & Chen, F., 2014. Palaeosol development in the Chinese Loess Plateau as an indicator of the strength of the East Asian summer monsoon: Evidence for a mid-Holocene maximum. Quaternary International, 334, 155–164.

Wanner, H., Solomina, O., Grosjean, M., Ritz, S. P., & Jetel, M., 2011. Structure and origin of Holocene cold events. Quaternary Science Reviews, 30(21), 3109–3123.

Wen, R.L., Xiao, J.L., Chang, Z.G., Zhai, D.Y., Xu, Q.H., Li, Y.C., Itoh, S., 2010. Holocene precipitation and temperature variations in the East Asian monsoonal margin from pollen data from Hulun Lake in northeastern Inner Mongolia, China. Boreas, 39, 262–272.

Wurster, C.M. and Patterson, W.P. 2001. Late Holocene climate change for the eastern interior United States. evidence from highresolution 6180 value of marital otoliths. Palaeogeography Palaeoclimatology Palaeoecology, 170, 81–100.

Xiao, J.L., Xu, Q.H., Nakamura, T., Yang, X.L., Liang, W.D., Inouchi, Y., 2004. Holocene vegetation variation in the Daihai Lake region of north-central China: a direct indication of the Asian monsoon climatic history. Quaternary Science Reviews, 23, 1669–1679.

Yang, S. L., and Ding, Z. L., 2004. Comparison of particle size characteristics of the Tertiary 'red clay'and Pleistocene loess in the Chinese Loess Plateau: implications for origin and sources of the 'red clay'. Sedimentology, 51(1), 77–93.

Yang, X.P., Scuderi, L., Paillou, P., Liu, Z.T., Li, H.W., Ren, X.Z., 2011. Quaternary environmental changes in the drylands of China-a critical review. Quaternary Science Reviews, 30, 3219–3233.

Yu, L., and Oldfield, F., 1989. A multivariate mixing model for identifying sediment source from magnetic measurements, Quaternary Research, 32, 168–181.

Yu, L., Nai'ang, W., Zhuolun, L., Zhou, X. and Chengqi, Z., 2012. Holocene climate cycles in northwest margin of Asian monsoon. Chinese geographical science, 22(4), 450-461.

Yu, Y., Yang, T., Li, J., Liu, J., An, C., Liu, X., Fan, Z., Lu, Z., Li, Y. and Su, X., 2006. Millennial-scale Holocene climate variability in the NW China drylands and links to the tropical

Clim. Past Discuss., doi:10.5194/cp-2017-10, 2017
Manuscript under review for journal Clim. Past
Published: 31 January 2017

Climate of the Past Discussions
Open Access

Pacific and the North Atlantic. Palaeogeography, Palaeoclimatology, Palaeoecology, 233(1), 149-162.

Zhao, C., Yu, Z., Zhao, Y., Ito, E., Kodama, K.P. and Chen, F., 2010. Holocene millennial-scale climate variations documented by multiple lake-level proxies in sediment cores from Hurleg Lake, Northwest China. Journal of Paleolimnology, 44(4), 995-1008.

Zhao, H., Chen, F. H., Li, S. H., Wintle, A. G., Fan, Y. X., & Xia, D. S., 2007. A record of Holocene climate change in the Guanzhong Basin, China, based on optical dating of a loess-palaeosol sequence. The Holocene, 17(7), 1015–1022.

Zhao, Y., and Yu, Z., 2012. Vegetation response to Holocene climate change in East Asian monsoon-margin region. Earth-Science Reviews, 113(1), 1–10.

Zhou, W.J., and An, Z.S., 1994. Stratigraphic divisions of the Holocene loess in China. Radiocarbon, 36, 37–45.

Zhou, S.Z., Chen, F.H., and Pan, B.T., 1991. Environmental changes during the Holocene in the Western China on millennial timescale. The Holocene, 1, 151–56.

Zhou, W.J., Yu, S.-Y., Georges, B., Kukla, G.J., Jull, A.J.T., Xian, F., Xiao, J.Y., Colman, S.M., Yu, H.G., Liu, Z., Kong, X.H., 2010. Postglacial changes in the Asian summer monsoon system: a pollen record from the eastern margin of the Tibetan Plateau. Boreas, 39, 528–539.

Zhu, Z.D., Liu, S., He, R.Z., 1982. Deserts evolution in the historic time, Physical Geography of China. Historic Geography, 6, 249–253.

Clim. Past Discuss., doi:10.5194/cp-2017-10, 2017
Manuscript under review for journal Clim. Past
Published: 31 January 2017

Figure captions

Figure 1. Top: satellite image map showing the location of the studied areas (red star) and the other sites discussed in the text: 1– Hongyuan peatland; 2– Yaozhou; 3– Jinjie; 4– Daihai Lake; 5– Hulun Lake; 6– Lake Baikal; 7– Burdukovo. Bottom: geographic location of the Yaozhou (YZ) and Jinjie (JJ) studied areas in the Chinese Loess Plateau.

Figure 2. Top: examples of temperature dependent magnetic susceptibility for the samples from YZ3 section (loess; sample 205 and soil; sample 150). Arrows represent heating (red line) and cooling (blue line) directions. Magnetic susceptibility is measured in the air; therefore increasing values due to formation of new magnetic minerals above 600°C is not shown. Bottom: representative hysteresis loops of the samples from YZ3 section (loess; sample 50 and soil; sample 250).

Figure 3. Day plot of the hysteresis parameters (based on Dunlop, 2002) for YZ3 (triangles), JJ1 (diamonds), and JJ3 (circles) sections. SD– single domain; PSD– pseudo-single domain; and MD– multidomain.

Figure 4. Stratigraphy and magnetic concentration parameters of the YZ1 section. χ_{lf}– low frequency magnetic susceptibility (10^{-6} m^3 kg^{-1}); FD (%) – frequency dependence parameter; χ_{ARM}– anhysteric remanent magnetization (10^{-6} m^3 kg^{-1}); and SIRM– saturation isothermal remanent magnetization (10^{-6} Am^2 kg^{-1}). Horizontal grey bars denote soil horizons, interpreted as relatively warm-wet intervals.

Figure 5. Stratigraphy and magnetic concentration parameters of the YZ2 section. Same abbreviations as in Figure 4.

Figure 6. Stratigraphy and magnetic concentration parameters of the YZ3 section. Same abbreviations as in Figure 4.

Figure 7. Stratigraphy and magnetic concentration parameters of the JJ1 section. Same abbreviations as in Figure 4.

Figure 8. Stratigraphy and magnetic concentration parameters of the JJ3 section. Same abbreviations as in Figure 4.

Figure 9. Stratigraphy and analytic data for the YZ1 section. χ_{lf}– low frequency magnetic susceptibility (10^{-6} m^3 kg^{-1}); MD– median sedimentary grain size (μm); χ_{ARM}/χ_{lf}– magnetic grain size parameter (unitless); and $\chi_{ARM}/SIRM$– magnetic grain size parameter (10^{-4} mA^{-1}). Horizontal grey bars denote soil horizons, interpreted as relatively warm-wet intervals.

Figure 10. Stratigraphy and analytic data for the YZ2 section. Same abbreviations as in Figure 9.

Figure 11. Stratigraphy and analytic data for the YZ3 section. Same abbreviations as in Figure 9.

Figure 12. Stratigraphy and analytic data for the JJ1 section. Same abbreviations as in Figure 9.

Figure 13. Stratigraphy and analytic data for the JJ3 section. Same abbreviations as in Figure 9.

Figure 14. Comparison of Holocene paleoclimate records in China (from south to north): total tree pollen percentage at Hongyuan peatland (Zhou et al., 2010); χ_{lf}– low frequency magnetic susceptibility (10^{-6} m^3 kg^{-1}) for YZ3 section (this study); χ_{lf} (10^{-6} m^3 kg^{-1}) for JJ3 section (this study); total tree pollen percentage at Daihai Lake (Xiao et al., 2004); and total tree pollen percentage at Hulun Lake (Wen et al., 2010). Locations of these areas are shown in Figure 1. Grey horizontal bars represent the warm-wet climatic intervals based on the record of this study.

Figure 15. Regional and global correlations (from south to north): χ_{lf}– low frequency magnetic susceptibility (10^{-6} m^3 kg^{-1}) for YZ3 section (this study); χ_{lf} (10^{-6} m^3 kg^{-1}) for JJ3 section (this study); Lake Baikal δO^{18} profile linked to mass-balancing isotope measurements in per mil deviations from VSMOW (Vienna Standard Mean Ocean Water) (Mackay et al., 2011); frequency dependence (FD) parameter from loess section of Burdukovo in Siberia (Kravchinsky et al., 2013); temperature variations (°C) in the northern hemisphere (relative to mean temperature during 1960–1980) averaged from multiple published sources (McMichael, 2012); and Drift Ice Indices Stack from North Atlantic (Bond et al., 2001). See Figure 1 for the locations. Grey horizontal bars indicate the warm-wet climatic intervals based on the record of this study.

Clim. Past Discuss., doi:10.5194/cp-2017-10, 2017
Manuscript under review for journal Clim. Past
Published: 31 January 2017

Climate of the Past Discussions

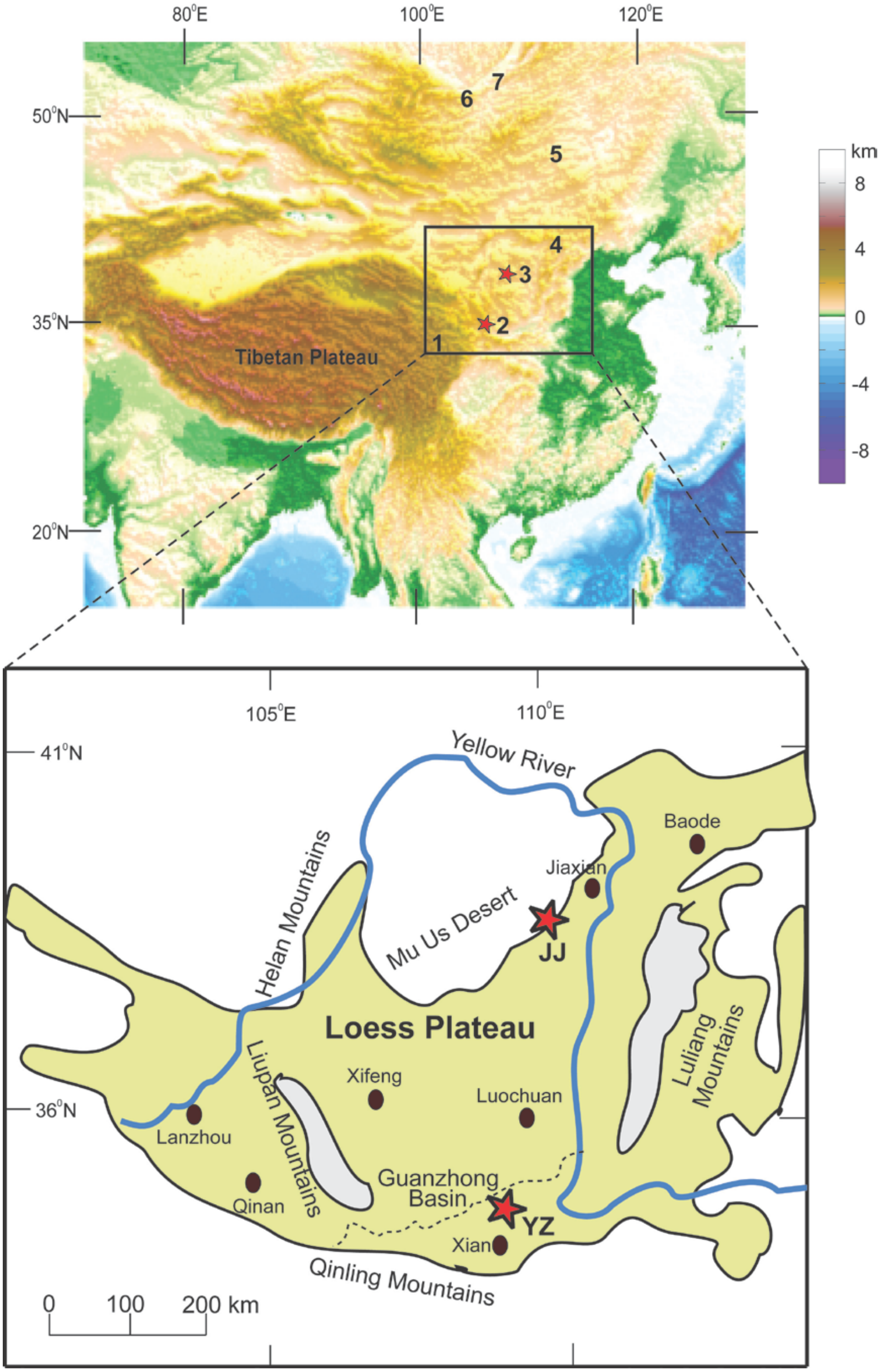

Clim. Past Discuss., doi:10.5194/cp-2017-10, 2017
Manuscript under review for journal Clim. Past
Published: 31 January 2017

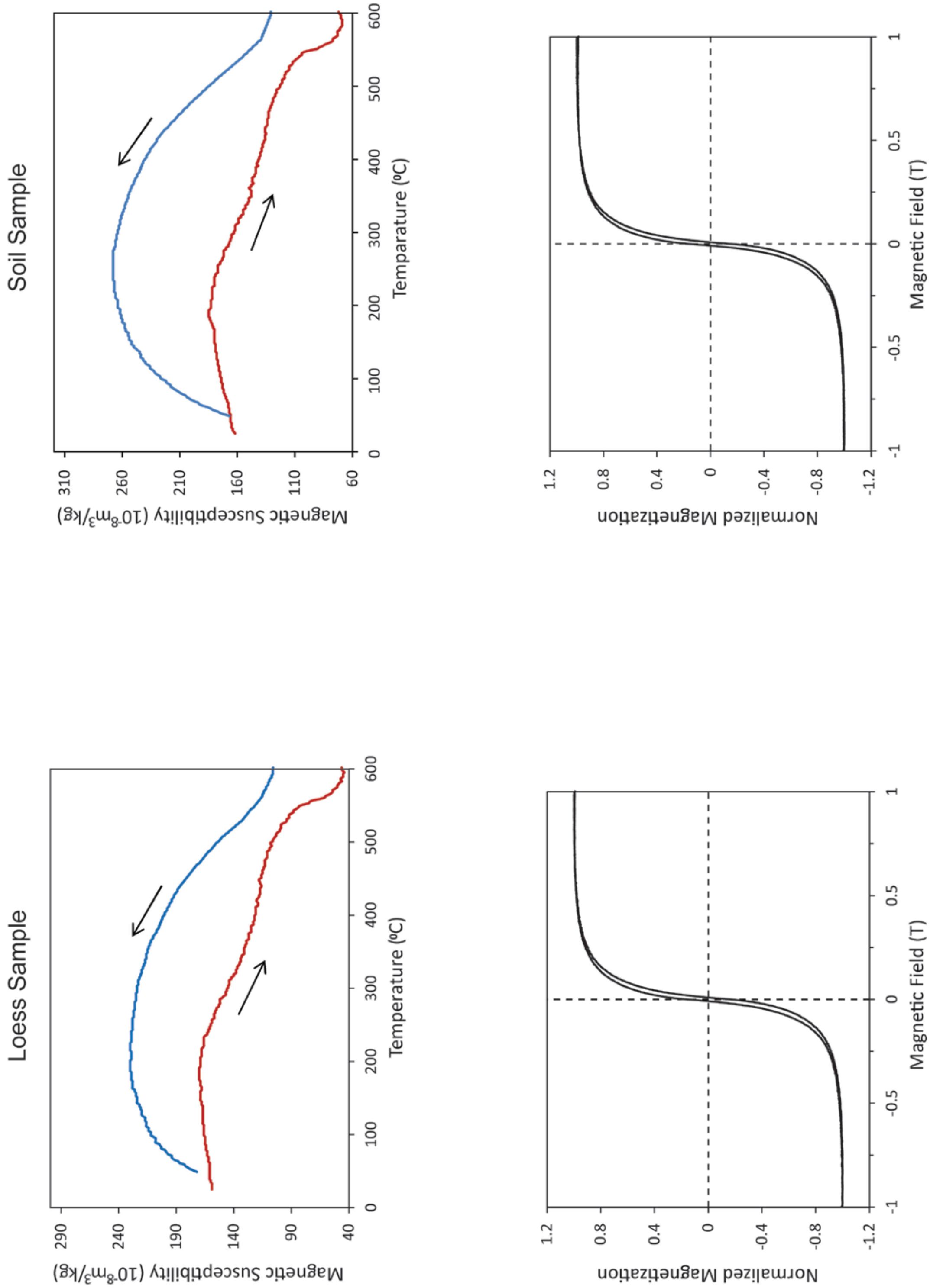

Clim. Past Discuss., doi:10.5194/cp-2017-10, 2017
Manuscript under review for journal Clim. Past
Published: 31 January 2017

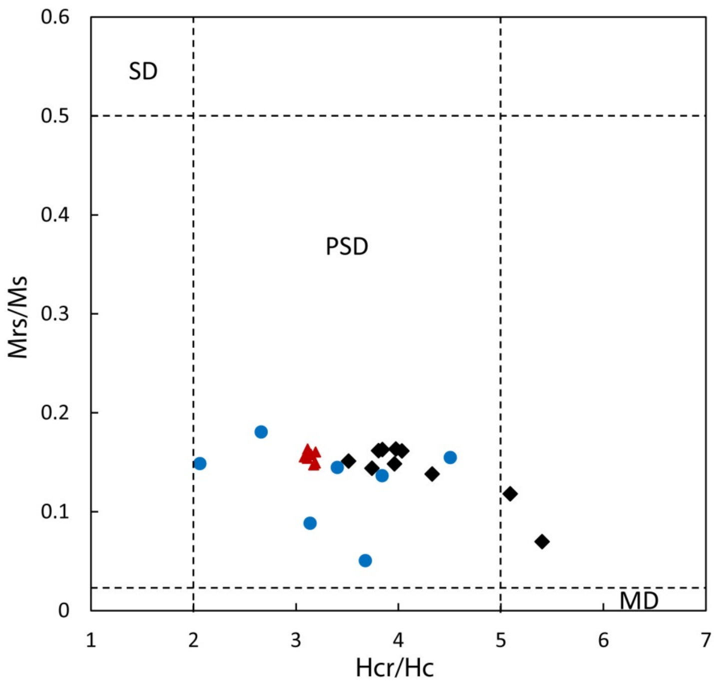

Clim. Past Discuss., doi:10.5194/cp-2017-10, 2017
Manuscript under review for journal Clim. Past
Published: 31 January 2017

Climate of the Past Discussions
Open Access
EGU

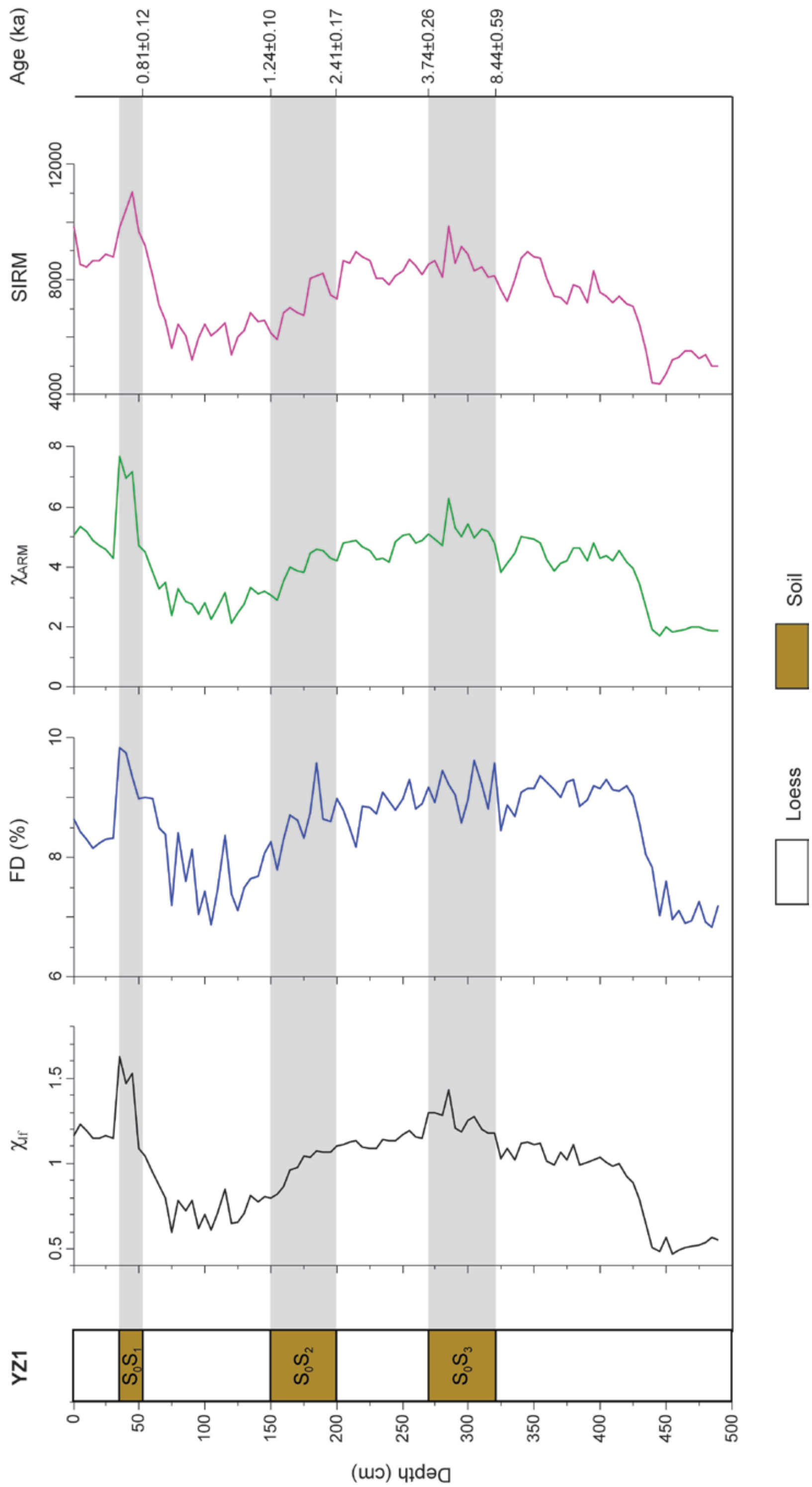

Clim. Past Discuss., doi:10.5194/cp-2017-10, 2017
Manuscript under review for journal Clim. Past
Published: 31 January 2017

Climate of the Past Discussions

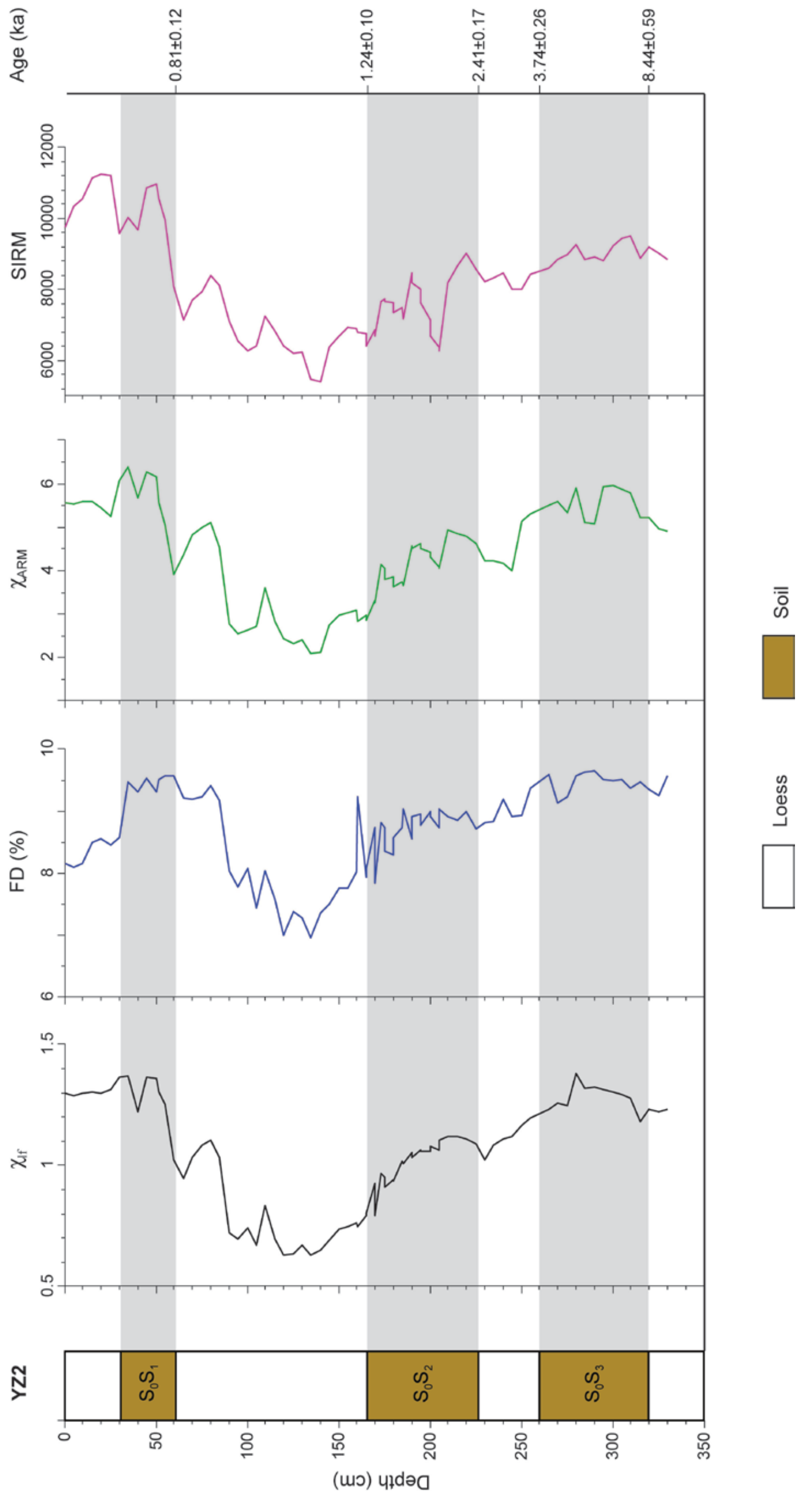

Clim. Past Discuss., doi:10.5194/cp-2017-10, 2017
Manuscript under review for journal Clim. Past
Published: 31 January 2017

Climate of the Past Discussions
Open Access

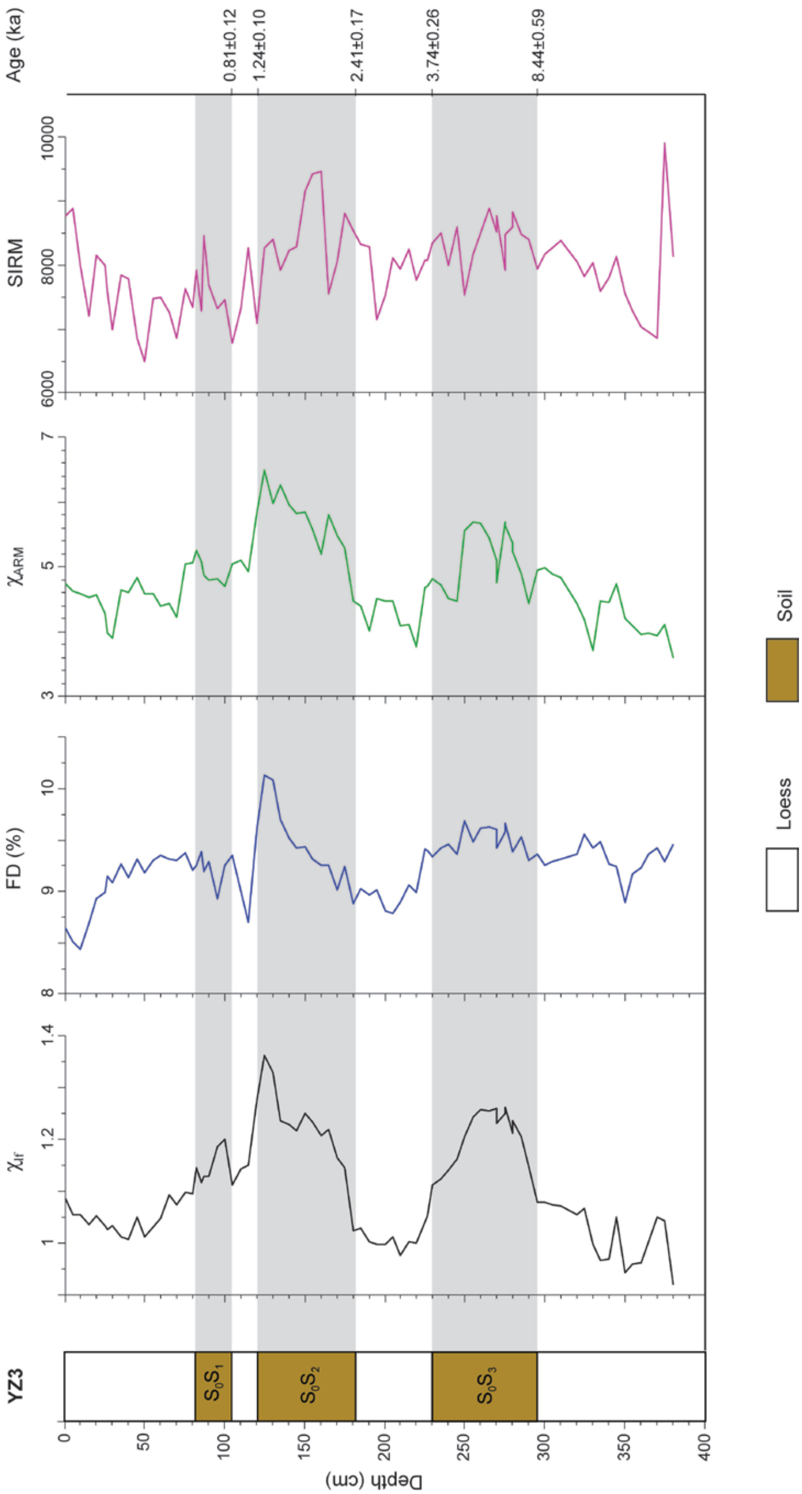

Clim. Past Discuss., doi:10.5194/cp-2017-10, 2017
Manuscript under review for journal Clim. Past
Published: 31 January 2017

Climate of the Past Discussions
Open Access
EGU

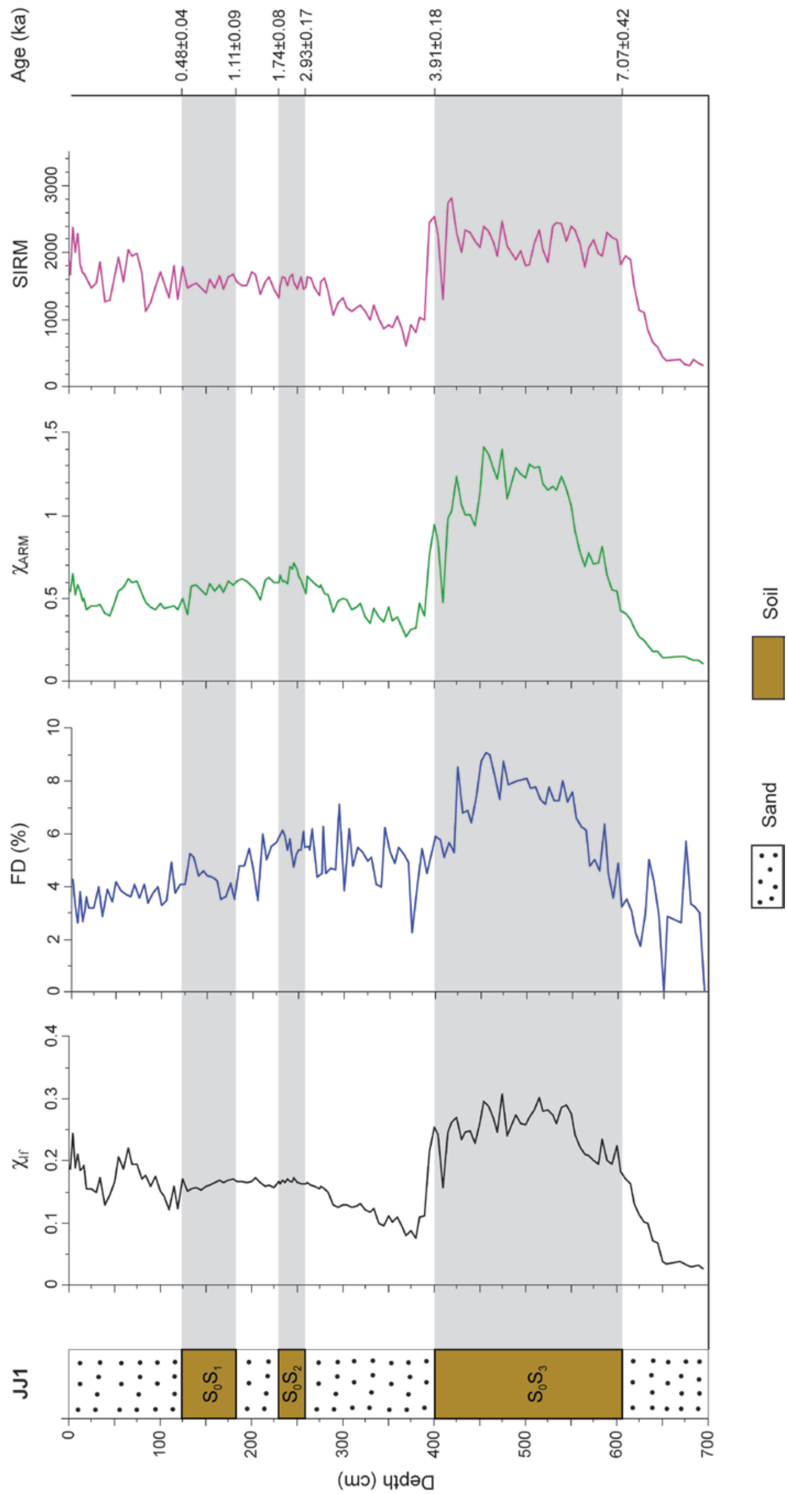

Clim. Past Discuss., doi:10.5194/cp-2017-10, 2017
Manuscript under review for journal Clim. Past
Published: 31 January 2017

Climate of the Past Discussions
Open Access

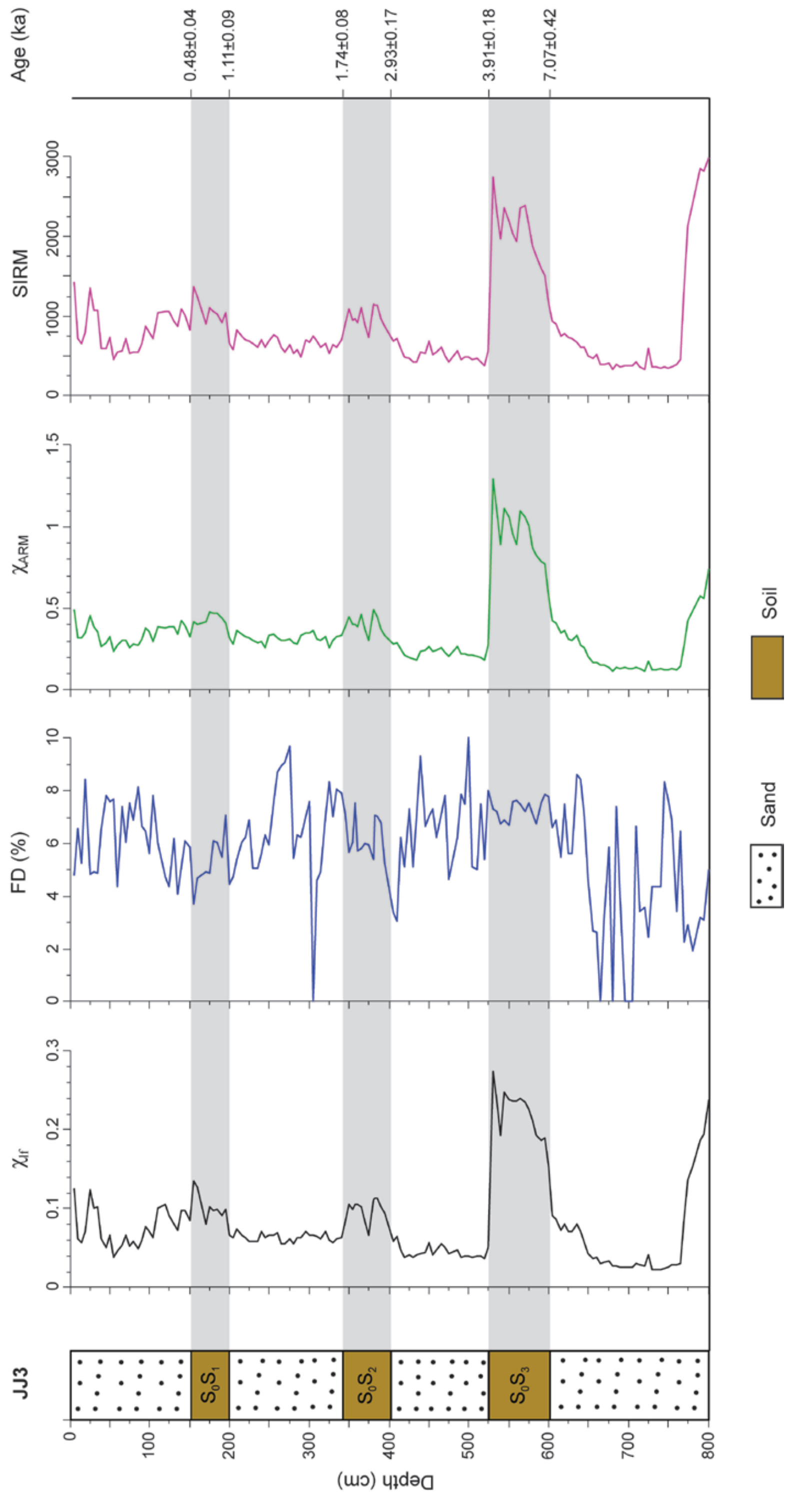

Clim. Past Discuss., doi:10.5194/cp-2017-10, 2017
Manuscript under review for journal Clim. Past
Published: 31 January 2017

Climate of the Past Discussions

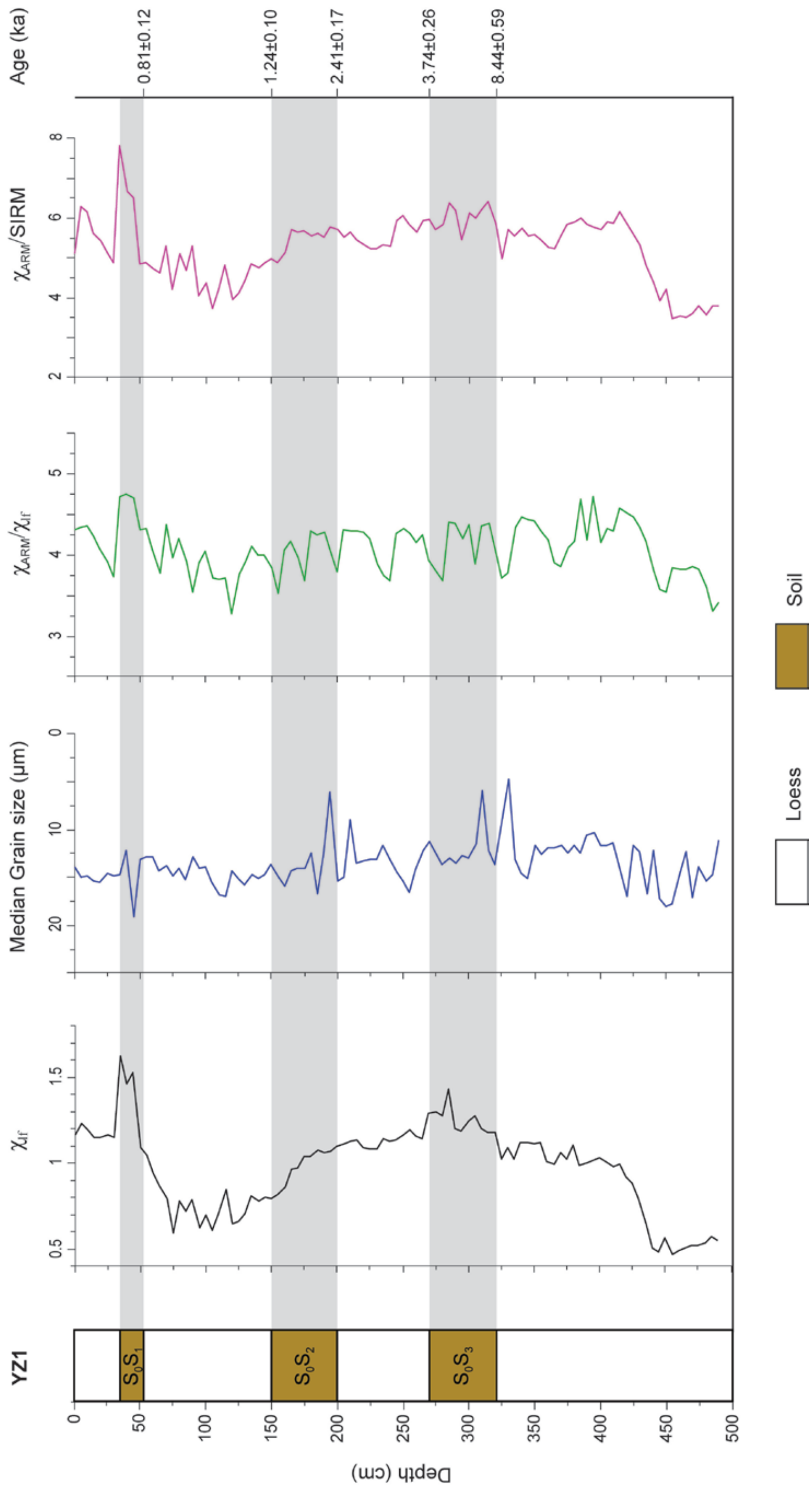

Clim. Past Discuss., doi:10.5194/cp-2017-10, 2017
Manuscript under review for journal Clim. Past
Published: 31 January 2017

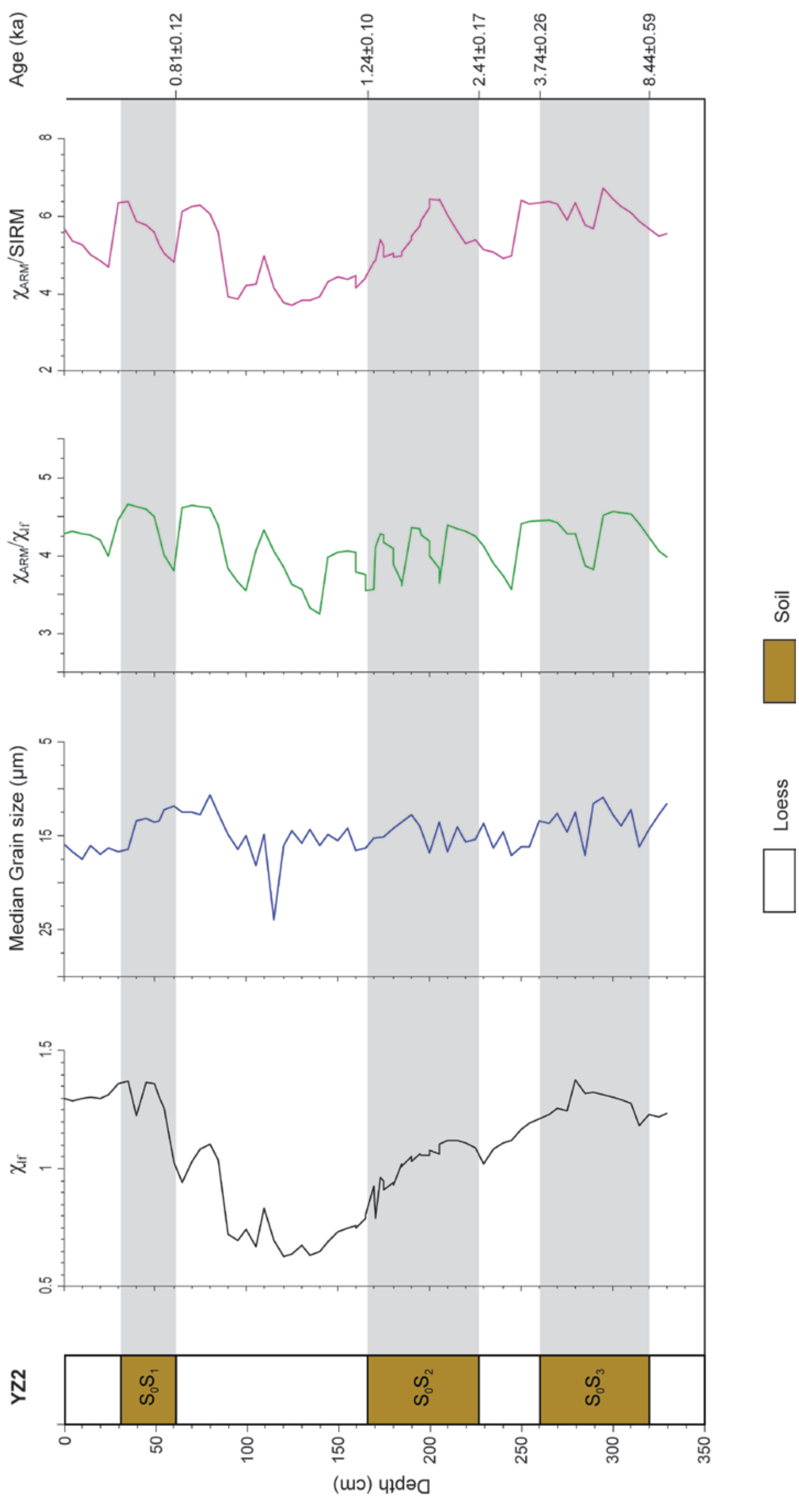

Clim. Past Discuss., doi:10.5194/cp-2017-10, 2017
Manuscript under review for journal Clim. Past
Published: 31 January 2017

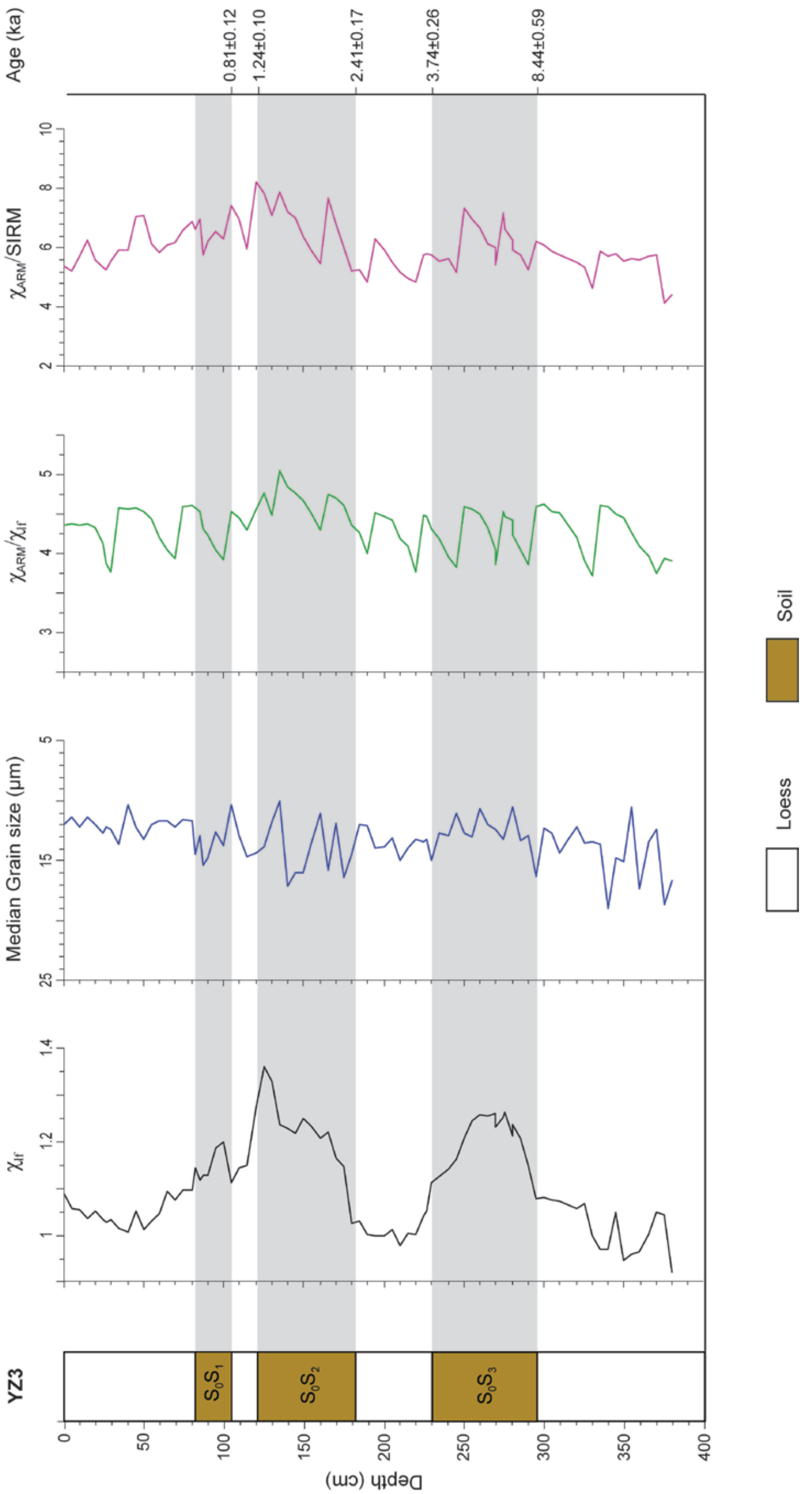

Clim. Past Discuss., doi:10.5194/cp-2017-10, 2017
Manuscript under review for journal Clim. Past
Published: 31 January 2017

Climate of the Past
Discussions

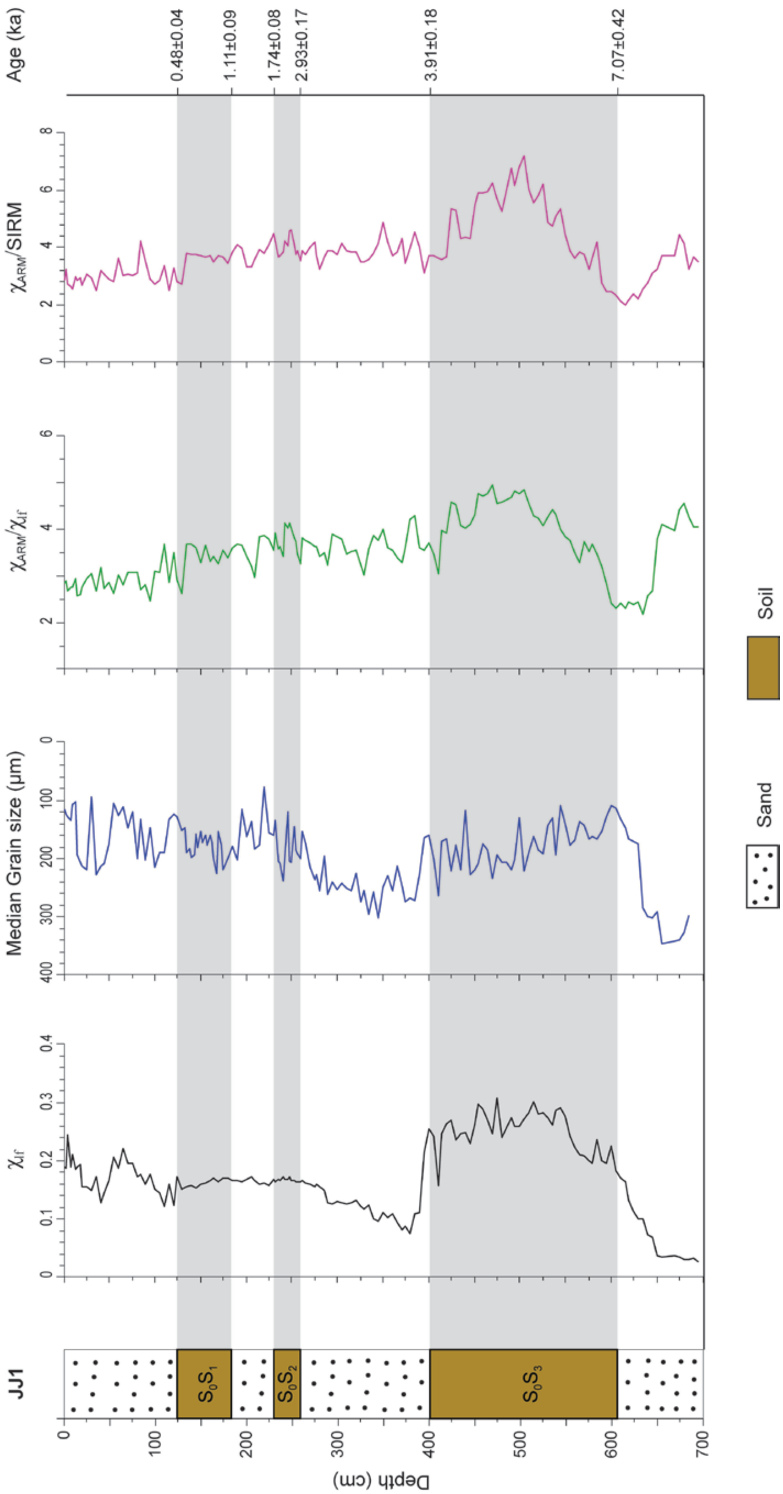

Clim. Past Discuss., doi:10.5194/cp-2017-10, 2017
Manuscript under review for journal Clim. Past
Published: 31 January 2017

Climate of the Past
Discussions
Open Access

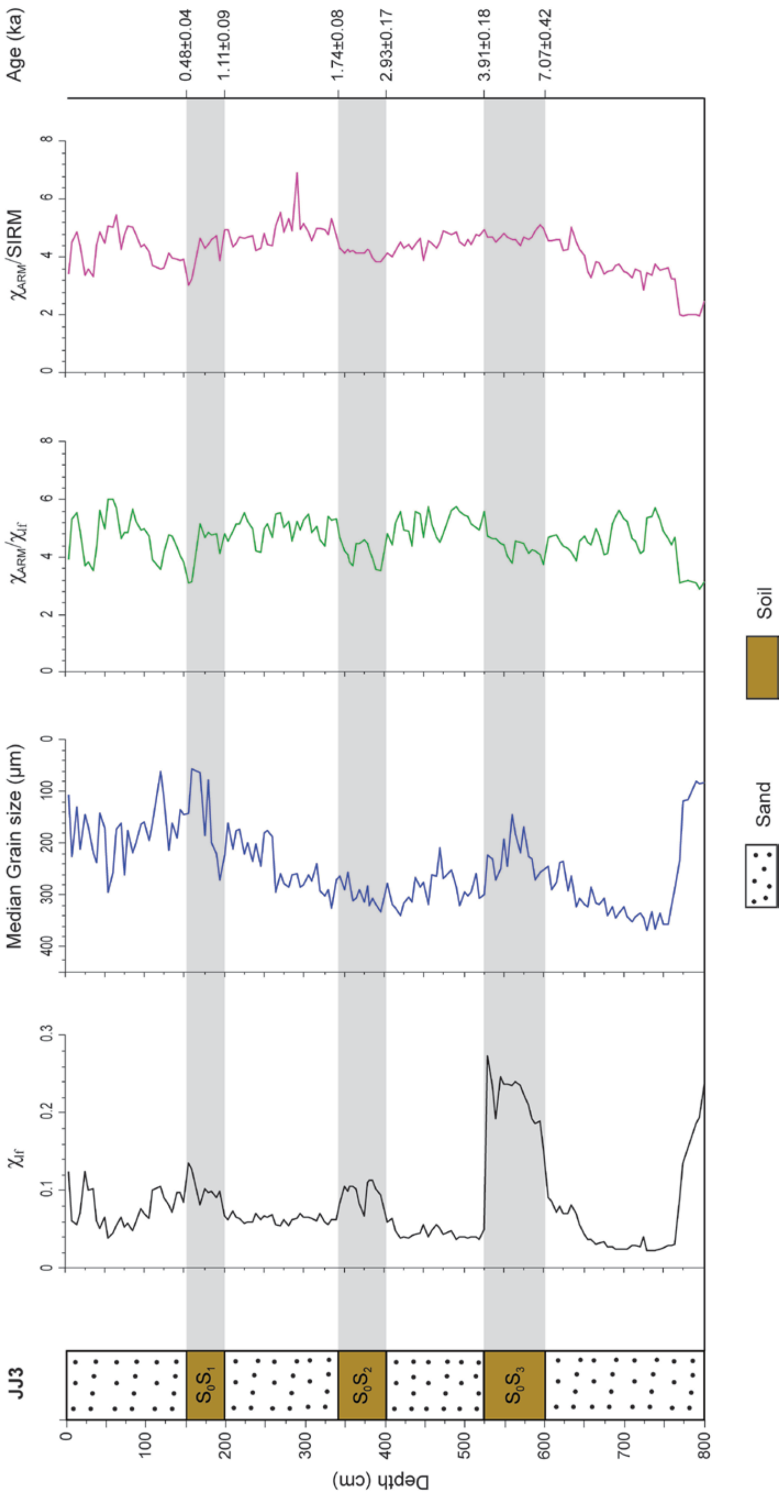

Clim. Past Discuss., doi:10.5194/cp-2017-10, 2017
Manuscript under review for journal Clim. Past
Published: 31 January 2017

Climate of the Past Discussions
Open Access

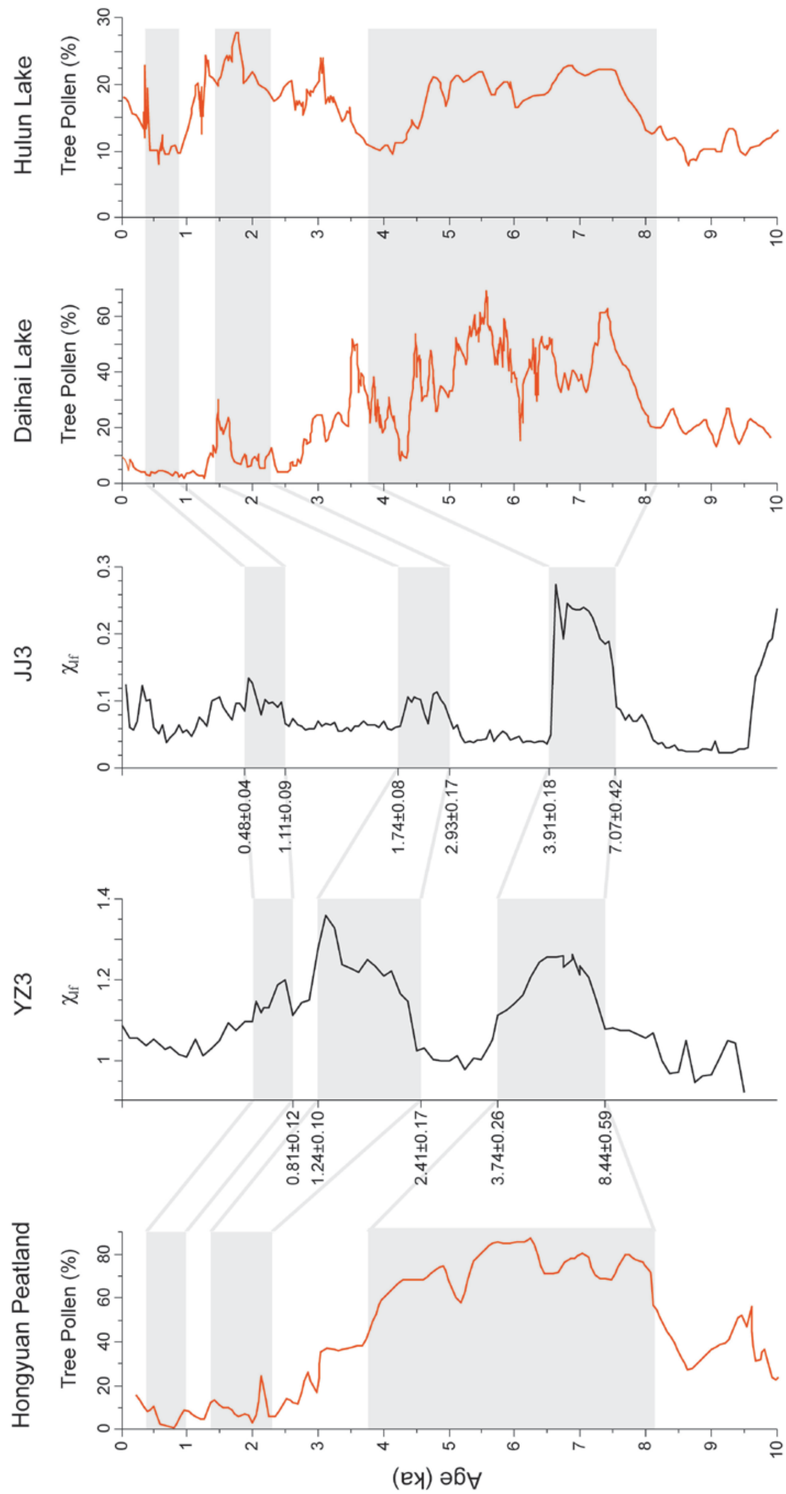

Clim. Past Discuss., doi:10.5194/cp-2017-10, 2017
Manuscript under review for journal Clim. Past
Published: 31 January 2017

Climate of the Past
Discussions
Open Access